Powder Technology 390 (2021) 504–520

Contents lists available at ScienceDirect

Powder Technology

journal homepage: www.elsevier.com/locate/powtec

Effects of fixed wall and pebble size ratio on packing properties and contact force distribution in binary-sized pebble mixed beds at the maximum packing efficiency state

Yongjin Feng, Baoping Gong *, Hao Cheng, Long Wang, Xiaoyu Wang

Southwestern Institute of Physics, P.O. Box 432, Chengdu 610041, PR China

ARTICLE INFO

Article history:
Received 27 January 2021
Received in revised form 20 May 2021
Accepted 30 May 2021
Available online 06 June 2021

Keywords:
Pebble size ratio
Wall effect
Maximum packing efficiency state
Porosity
Radial distribution function
Contact force

ABSTRACT

The binary-sized pebble mixed beds at the maximum packing efficiency state were numerical simulated by the DEM simulation to investigate the effect of fixed wall and pebble size ratios. The evolution of the distribution of packing fraction and porosity, radial distribution function and contact force were given and analyzed with emphasis on the effects of the fixed wall and pebble size ratio. The results showed that the fixed wall will result in a reduction of average packing fraction and an obvious wall effect in local porosity distribution. With the increase of the pebble size ratio, the volume fraction of the wall affected regions gradually decrease. The variation of the local packing fraction of the binary-sized pebble bed is mainly determined by the partial packing fraction of large pebbles and the partial packing fraction of small pebbles, respectively, in the regions close to the fixed wall. Furthermore, the fixed wall has little effect on the radial distribution function and contact force. However, the pebble size ratios have great influence on the radial distribution function and the contact force in binary-sized pebble bed at the maximum packing efficiency state. With the increase of the pebble size ratio, the radial distribution functions of the whole pebble beds are consistent with that of small pebbles, and approach to that of the mono-sized pebble bed. In addition, with the increase of the pebble size ratio, a higher contact force can be obtained in pebble beds.

1. Introduction

Granular matters are ubiquitous in both nature and many industry systems, which consists of large amounts of discrete particles, such as, grain, sand, rock-fill, etc. in nature, and the fluidized bed, drying bed, catalytic bed, etc. in chemical system. In addition, the pebble bed has been used more and more widely in the nuclear reactor. Such as, in pebble-bed nuclear reactor the fuel and graphite are used in form of mono-sized pebbles [1,2]. In the nuclear fusion reactor, the tritium breeder materials and the neutron multiplier materials are used in form of monodisperse and binary pebbles in the tritium breeding blanket [3–15]. Many researchers have deeply investigated the packing behaviors of mono-sized pebble bed due to the widely application. In recent years, however, due to the advantages of the higher packing fraction and the larger effective thermal conductivity compared with mono-sized pebble bed [16], the binary-sized and poly-disperse pebble bed have been used more and more. Such as, the binary-sized beryllium pebbles at maximum packing efficiency state were used as neutron multiplier in HCCB TBM [3,7], the poly-disperse Li_4SiO_4 pebbles with the diameter of 0.25–0.65 mm were used as tritium breeder in the EU HCPB TBM [17–19]. Therefore, it is of great significance to investigate the effect of pebble size ratio on the packing fraction (or called packing density, packing factor) and porosity of binary-sized and poly-disperse pebble bed at maximum packing efficiency state for its applications in nuclear fusion reactor and other industrial system.

The previous results [20–37] show that the mechanical properties of binary-sized pebble beds are strongly related to the packing behaviors of the pebble bed, including the packing fraction, porosity, coordination number, contact force, and so forth. Thus, many experiments and simulations were carried out on the investigations of packing structures in binary-sized pebble bed [33–36,38–40]. The average packing fraction of binary-sized pebble bed have been experimentally determined in many literature [32,33,38,41–49] and several theoretical models for predicting the packing fraction of the binary-sized pebble beds have been proposed [46–50]. The results reported in the literature show that the average packing fraction of binary-sized pebble beds were affected obviously by the volume fraction of large pebble (VFL) and the pebble size ratio (SR), as shown in Fig. 1. With the increase of the VFL the packing fraction increases first and then decreases. The maximum packing fraction can be obtained at the VFL of 60–80% with different SR. In addition, the packing fraction increases rapidly as the SR increases

* Corresponding author.
E-mail addresses: gongbp@swip.ac.cn, gongbp@gmail.com (B. Gong).

https://doi.org/10.1016/j.powtec.2021.05.099
0032-5910/

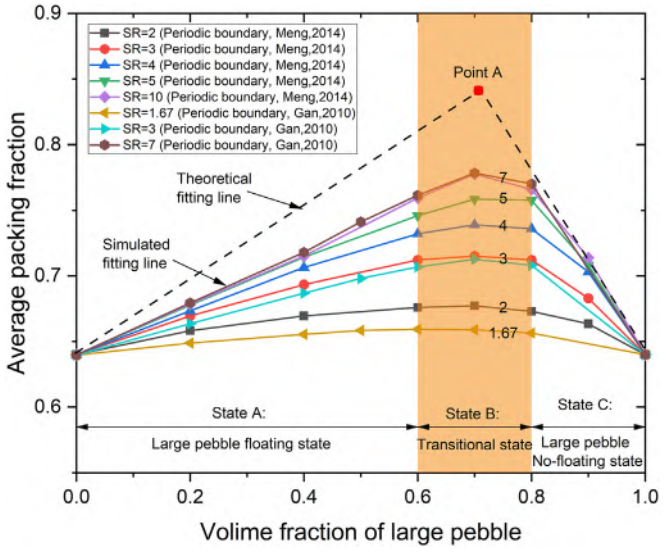

Fig. 1. The average packing fraction variation in binary-sized pebble mixed bed.

in the binary-sized pebble bed with constant VFL. Meng et al. [35] systematically investigated the packing properties of the binary-sized pebble bed with periodic boundary based on the numerical simulation by using a relaxation algorithm. In addition, the fixed wall has significant influences on packing behaviors and porosity distribution in pebble bed [51,52]. For example, Reimann et al. [51] investigated the mono-sized pebble packing in cylinder container with and without the inner cylinders. The results shown that the concave and convex wall have great influence on packing structure of mono-sized pebbles packed bed close to fixed walls, especially the radial porosity distribution. Dai et al. [52] investigated the structural dynamics of mono-sized pebble packing in confined cylinder during the mechanical vibration. The results show that the mechanical vibration brings a disorder-to-order transition and a granular crystallization was induced under the effect of the confined wall. However, most of the investigations were focused on the wall effect on the radial porosity variation in mono-sized pebble bed [51–54], the effect of fixed wall on the variation of the local porosity in binary-sized pebble bed are few reported.

Generally, there are three typical packing states in the binary-sized mixed pebble bed corresponding to the variation of the VFL [34,35,55–57], namely, the large pebble floating state, transitional packing state and no-floating packing state of large pebble. These three packing states correspond to the different VFL, as shown in Fig. 1. In the large pebble floating state, small pebbles occupy the most of the bed volume, whereas in the large pebble non-floating packing state, the large pebbles occupy the majority volume of the pebble bed and the small pebbles are filled in a part of the voids formed between large pebbles. Relative low average packing fraction and larger porosity can be observed in both the large pebble floating state and the large pebble non-floating state. While, in the transitional packing state, the gaps between large pebbles are fully filled up with small pebbles. The higher packing fraction and the minimum porosity are obtained generally in the transitional packing state. When the maximum packing fraction are obtained, the packing state can be called the maximum packing efficiency state. In addition, it is clear that in the large pebble floating and non-floating packing state, the contact force chains of binary-sized pebble bed are dominated by small pebbles and large pebbles respectively [34]. However, in the transitional packing state, it is difficult to distinguish whether the contact force chains in binary-sized pebble bed are dominated by small pebbles or large pebbles. Thus, more comprehensive investigations of the contact force distribution in binary-sized pebble bed are needed.

As far as the authors know, the majority of the studies of the packing properties of binary-sized pebble bed have focused on the effect of VFL and SR on average packing fraction [7,23–28,32–39,47–50]. Gan et al. [39] investigated the packing structures of the binary-sized pebble bed with different VFL and PSR by an extended random close packing algorithm for polydisperse particle packing. The results show that the maximum packing fraction can be obtained in the range of VFL between 0.6–0.8. A similar result can be observed in Meng et al.'s investigation [35]. Chen et al. [7] simulated the binary-sized pebble packing for mixed pebble beds of water-cooled ceramic breeder blanket. A packing fraction of more than 0.75 for $Li_2TiO_3/Be_{12}Ti$ mixed breeding pebble bed can be achieved with SR = 5 and VFL around 0.6–0.7. Reimann et al. [58] explored the packing structure of pebble packing in slender prismatic container. The packing structures were characterized by the packing fraction, coordination number, contact angle and Voronoi packing fraction. In addition, Dong et al. [59] explored the packing structures of the order to disorder transition within 2D binary-sized granular packing under vibration. However, few studies were carried out on the effects of pebble size ratio and the fixed wall effect on the local packing fraction variation close to fixed wall and the contact force distribution in three-dimensional binary-sized pebbles packed bed, especially at the maximum packing efficiency state. The existing results are also insufficient to comprehensively explain the effect of pebble size ratio on the radial distribution function and organization of binary-sized pebble bed.

Therefore, the effects of the pebble size ratio and the fixed wall on the inner packing structure and the contact force distribution of binary-sized pebbles densely packed beds are investigated by using discrete element method (DEM) simulation in this study. The binary-sized pebble mixtures are performed with different VFL and SR. The effect of pebble size ratio and fixed wall effect on the local porosity distribution, the radial distribution function and the contact force in binary-sized pebble mixed bed at the maximum packing efficiency state with different pebble size ratios (SR = 1,3,5,7) and side boundary condition (fixed side wall and periodic boundary) are also discussed to gain further insight into the packing properties of binary-sized fixed pebble bed.

2. Simulation methodology

2.1. Discrete element method

In this work, the Discrete Element Method (DEM), first introduced and by Cundall [60], was applied to model the packing of binary-sized spherical pebbles under gravity. Each pebble is considered as an independent element and the following assumptions are applied in the simulation: a) All the particle are absolute spherical pebbles; b) The material properties of spherical pebbles are uniform and isotropic; c) The pebbles are hard rigid sphere, only very small overlaps exist between two contact pebbles or between wall and pebble, which can be regarded as point contact; d) The contact force between two touched pebbles is calculated by the Hertz-Mindlin theory; e) In the process of pebble motion, the Coulomb Friction Law is applied to simulate the friction phenomenon between two contact pebbles and between wall and pebbles.

According to the overlap distance and the contact theory, the contact forces between two pebbles contact with each other are calculated circularly. Each pebble is tracked in the simulation. The collisions and the sliding between the pebbles and between wall and pebbles are all modeled. During the packing process, the motions of every pebbles confirm to the Newton's second law of motion. The pebble motions are driven by the contact forces from interactions with neighboring contact particles and the gravity. The details of the Hertz-Mindlin contact theory can be found in Ref. [60, 61].

2.2. Packing process and parameters

It is well known that the average packing fraction and the average porosity of the binary-sized pebble bed are affected obviously by the SR and the VFL, as shown in Fig. 1. The average packing fraction first increases gradually and then decreases rapidly with the increase of the VFL in the binary-sized pebble bed. A larger packing fraction can be obtained at the VFL of 60% ~ 80%. The point A represents the theoretical maximum packing efficiency state of binary-sized pebble packing. The maximum packing efficiency state of binary-sized pebble packed bed is defined as a dense packing state of binary-sized pebbles mixture that small pebbles are densely packed in the void formed among the large pebbles, as a result, the maximum packing fraction can be obtained at this pebble packing state [34]. However, during the packing process in reality, the theoretical maximum packing efficiency state is always difficult to be achieved. The packing fraction of the binary-sized pebble mixed bed is actually always lower than that at theoretical maximum packing efficiency state. Thus, in realistic packing experiment, the packing state with maximum packing fraction can be called the maximum packing efficiency state in many packing experiments, which is described as the packing state of binary-sized pebble bed in which the small pebbles are fully filled as many as possible and densely packed in the gaps among large pebbles in realistic packing experiment.

Table 1
Parameters used in the DEM simulation.

Property	Symbol	Pebble (Li_4SiO_4 [8–10])	Wall (CLF-1 steel [62])
Density	ρ(g/cm^3)	2.323	–
Young's modulus	Y (GPa)	90	225
Poisson ratio	v	0.24	0.33
Friction coefficient for pebble-pebble	μ_{pp}	0.1	–
Friction coefficient for pebble-wall	μ_{pw}	0.1	
Coefficient of restitution	e	0.9	
Time-step	Δt (s)	1e-7	–
Diameter of small pebble	d_s(mm)	1	–
Diameter of large pebble	d_L(mm)	1, 3, 5, 7	–

In order to analyze the packing behaviors of binary-sized pebble bed. The simulations, repeated at least 3 times, were performed with different SR and VFL to achieve the maximum packing efficiency state. The results of average packing fraction are shown in Fig. 2. It is clearly and noticeably show that the maximum packing efficiency states were obtained at the VFL of 70%, which are agreed well with the previous investigation reported in literature [35,39].

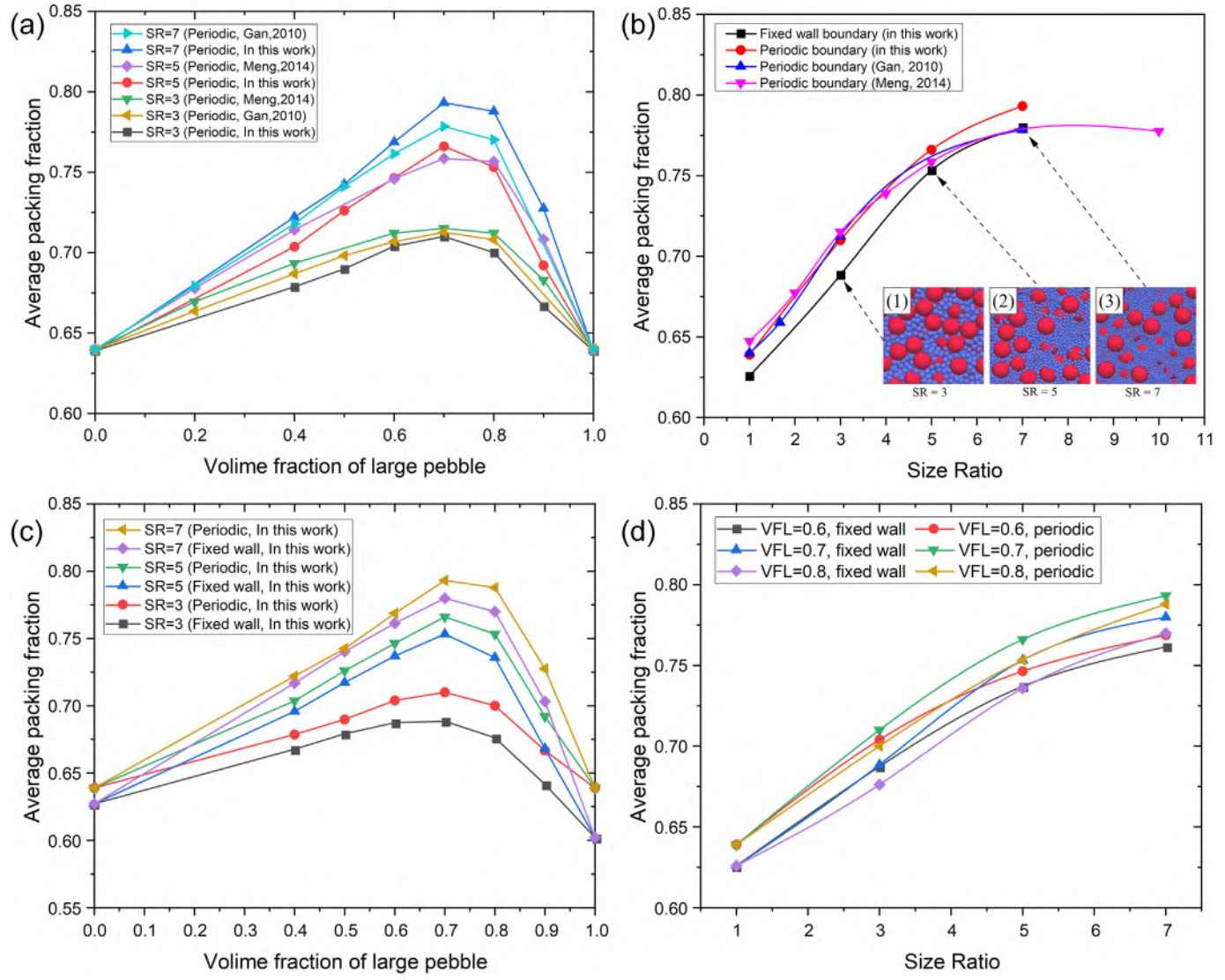

Fig. 2. Average packing fraction of binary-mixed pebble bed various as volume fraction of large pebble and size ratio: a) and b) compared with literature results (Meng, et al. [30] and Gan, et al. [34]); c) and d) fixed wall effect.

Thus, the following analysis were focused on the packing performance of binary-sized pebble bed at the VFL of 70%. In addition, the Li_4SiO_4 pebble, which is used as tritium breeder of a typical solid tritium breeder blanket of fusion reactor [3–11], is employed as a case to investigate the effect of pebble size ratio and fixed wall on packing properties and contact force in binary mixed pebble bed at maximum packing efficiency state in this study. The parameters of pebble used in this study are listed in Table 1 by referring the literature [8–11,62].

The results of Meng et al. [35] and McGeary et al. [63] indicated that the pebble size ratio of 1–7 have an obvious effect on the packing behaviors of binary-sized pebble bed. Thus, four kinds of pebble size ratios (SR = 1, 3, 5, 7) are selected. When SR =1, the pebble bed is equivalent to mono-sized pebble bed. Thus, the packing of mono-sized pebbles was also simulated and compared with results from literature to validate the simulation in this study. For the binary-sized pebble packing, the small pebble diameter was selected as 1 mm, the large pebble diameters were 1 mm, 3 mm, 5 mm, 7 mm, respectively. In addition, in order to reveal the fixed wall effect on the packing structures of the binary-sized pebble beds, the fixed side wall and periodic boundary along the X/Y directions (side wall directions) were adopted in this study. Along the *Z*-axial direction, the fixed wall was also applied at the bottom plane in all simulations to support the gravity of pebble bed. The dimension of the pebble bed along the X-axis and Y-axis directions are 10 times of the large pebble diameter to clearly show the influence of wall effect on the packing structure of binary-sized pebble bed. In addition, since the gravity always exists in many application fields of granular system, the gravity with acceleration of $g = 9.81\ m/s^2$ was also applied in the simulation.

The pebbles were inserted into the container in batches under gravity. The packing processes of the binary mixed pebbles are as follow: First, in the top zone of the container, a certain number of pebbles were generated randomly according to the predefined pebble size and pebble proportion with no overlaps between pebbles. Then, the generated pebbles began to freely fall under the gravity. Simultaneously, a variable number of binary-sized spherical pebbles will be regenerated in batches in the top region of the container at every specified time-step. During the packing process, the pebble number in the bed will increases continuously. The collision, sliding, friction and rolling motion between pebbles will happen continuously and circularly. When the pebble bed height reaches a certain value of about $10d_L$, it will stop filling pebbles into the container. From that moment on, the kinetic energy of pebbles is dissipated gradually owing to the collision, sliding, friction and rolling process. Finally, under the interaction of the gravity, the contact force, friction interaction, and energy dissipation, the pebble reaches an equilibrium static state gradually. Pebbles are packed in the container randomly. At that time, the sum kinetic energy of all pebbles in bed is about $\sim 10^{-14}$ J. The pebbles can be considered as neither translating nor rotating. The further analysis of packing properties can be carried out.

3. Results and discussion

3.1. Effects of pebble size ratio and fixed wall on packing fraction and porosity distribution

3.1.1. Average packing fraction

Although a large number of experimental and simulation investigations of the average packing fraction of binary-sized pebble mixed bed have been reported, in this study, the average packing fractions of binary-sized pebble mixed beds were still calculated and presented here to compare with results from literature [35,39] and validate the

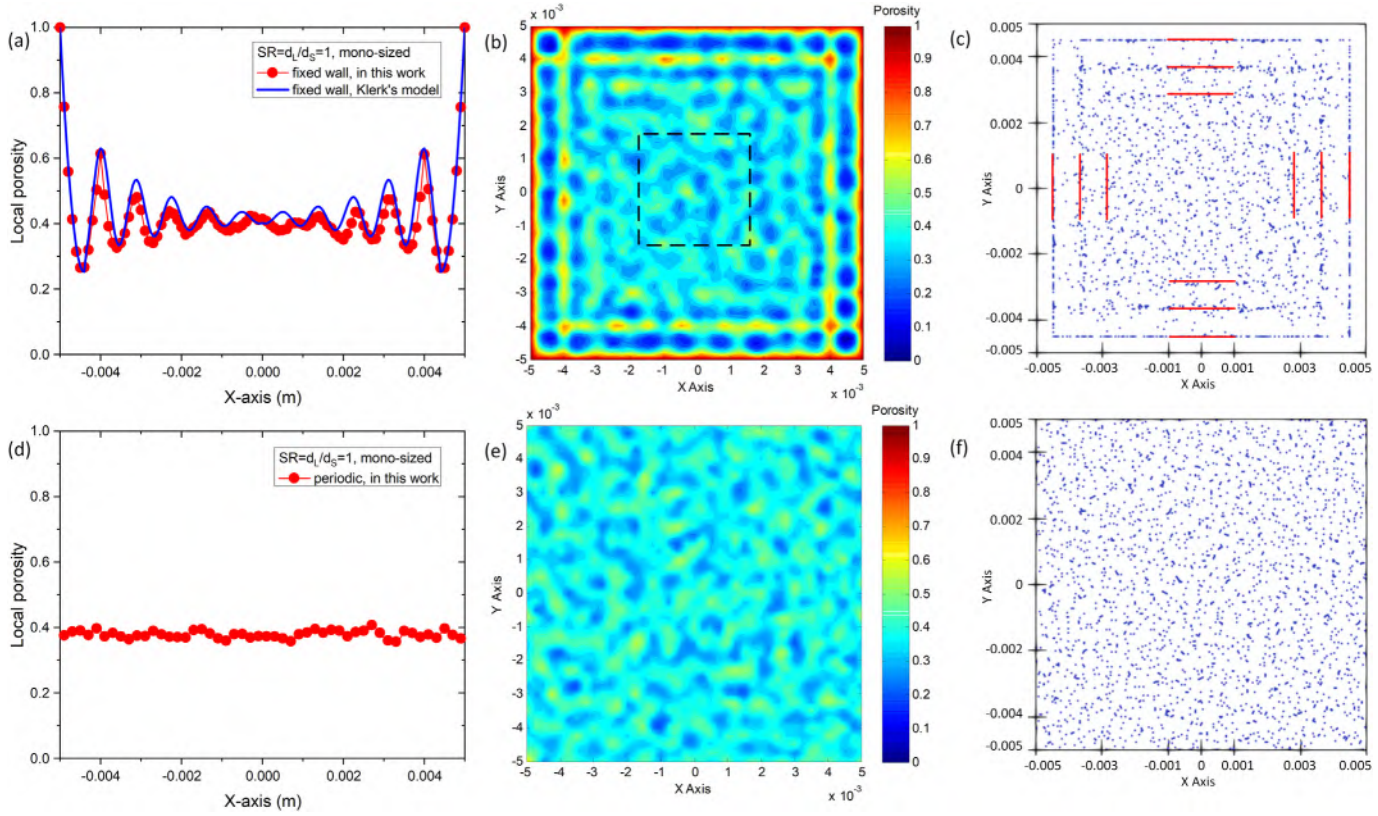

Fig. 3. Fix wall effect on the local porosity variation and pebble center distribution in mono-sized pebble bed with fixed wall and periodic boundary.

simulation in this work, as shown in Fig. 2. It is well known that the average packing fraction of binary-sized pebble bed is significantly affected by pebble size ratio and volume fraction of large pebble. In binary-sized pebble bed without considering the fixed wall, the average packing fraction first increases gradually and then decreases rapidly with the increase of the VFL and also increase as the increase of the SR. The results gained in this study are agreement well with that from literature [35,39], as shown in Fig. 2a and b.

Furthermore, Fig. 2c and d show the average packing fraction depends on the VFL and the SR in binary-sized pebble bed with fixed wall and periodic boundary in side. The results reveal that the fixed wall affects the packing fraction in binary-sized pebble bed, which will result in a relative lower average packing fraction compared with periodic boundary pebble bed. It can be clearly seen from the figure that the same variation trend of average packing fraction is obtained in binary-sized pebble beds with the fixed wall and the periodic boundary in this study. The average packing fraction of binary-sized pebble bed first increases gradually and then decreases quickly with the increase of the VFL. A relatively large packing fraction is obtained when the VFL in the range of 60% ~ 80%. The maximum average packing fraction of the binary-sized pebble mixed bed is achieved in the VFL of 70% in this study. At this time, the pebble bed reaches the maximum packing efficiency state. Thus, the discussion in following section is focused on the packing properties of pebble beds at the maximum packing efficiency state. In addition, when VFL is constant, as the pebble size ratio increases the average packing fraction increases significantly, as shown in Fig. 2d. For instance, the average packing fraction increases from 0.62–0.64 when the pebble size ratio is 1 to 0.76–0.8 when the pebble size ratio is 7 in binary-sized pebble bed in this study. The average packing fraction of pebble bed with fixed side wall is obviously smaller than that with periodic boundary, which is mainly due to the relative loose arrangement of pebble close to the fixed wall. The pebbles in the bed with periodic boundary are far away from the fixed wall. Without the effect of fixed wall, a higher packing fraction and a denser packing structure can be obtained. The effect of fixed wall on the packing properties of the binary-sized pebble mixed bed can be revealed in detail from the local porosity distribution of the pebble bed, which will be discussed in Section 3.1.2.

3.1.2. Local porosity distribution

The porosity of pebble bed is an important parameter to characterize the local packing structure of fixed pebble bed. The porosity distribution inside pebble bed affects the flow behaviors of fluid (liquid and gas) in pebble bed, such as pressure drop, velocity distribution, pressure distribution, mass distribution, and so forth. Therefore, in this section, we focused on the investigation of the effects of the pebble size ratio and fixed wall on the local porosity in binary-sized pebble mixed bed at the maximum packing efficiency state.

When SR = 1, the pebble beds can be regarded as mono-sized pebble beds. Fig. 3 provides the local porosity distribution and pebble center distribution in mono-sized pebble beds with fixed wall and periodic boundary. Along the *x*-axis directions, the axial local porosity is almost stable in the whole pebble bed with periodic boundary. Only a slight variation can be observed around the average porosity (see Fig. 3d.), which is mainly caused by the pebble random packing. It can be seen from the contour map of porosity distribution and the figure of pebble center distribution (pebble center was projected into the bottom plane) that the uniform packing structure can be obtained in the

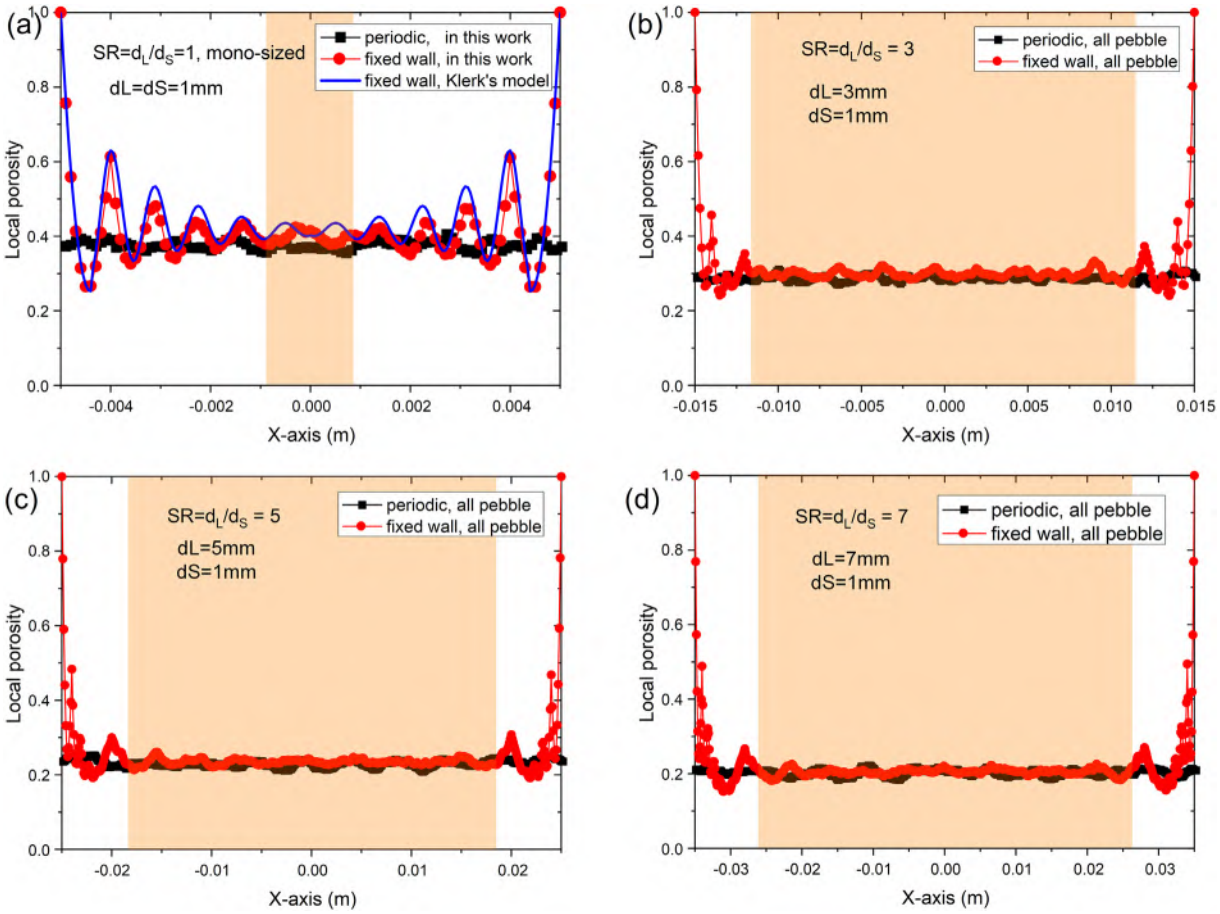

Fig. 4. Effect of pebble size ratio and fixed wall on the axial local porosity distribution in binary-sized pebble bed: (a) SR = 1, (b) SR = 3, (c) SR =5, (d) SR = 7.

binary-sized pebble mixed bed with periodic boundary, which corresponds to the results observed in Fig. 3d and e.

However, when the pebbles packed in a container with fixed wall boundary, the axial local porosity shows a drastic fluctuation characteristic in the near wall region. With the increase of the distance to the fixed wall, the fluctuations are gradually damped and the local porosity gradually approach to a constant value, which can also be observed in the porosity distribution contour in Fig. 3b. Only in the inner region of the bed with fixed wall, uniform distribution of local porosity similar to that of the periodic boundary pebble bed can be observed. Moreover, the wall effect on packing structure can also be indicated in the pebble center distribution (Fig. 3c). A layered pebble center distribution parallel to the wall can be observed near the fixed wall. While, in the inner zone, pebble center is distributed randomly and uniformly. This is mainly because the pebble packing must conform to the wall's curvature in container vessels. The packing structures and the arrangements of pebbles are relatively regular and loose due to the influence of container wall, which will result in the greater porosity near the wall of the container vessels compared the inner bulk region of the beds. Furthermore, adjacent to the fixed wall, the local porosity approach to 1, since each pebble can only touch the wall with point contact. With the increase of the distance to the wall, the amplitude of the porosity fluctuations is gradually damped. In the inner region of the pebble bed, which is far from the wall, the packing arrangements are almost not affected by the wall effect. a relative constant porosity can be observed. The wall effect regions are limited in the range of $4d \sim 5d$ close to the fixed wall in the mono-sized pebble bed. Moreover, the local porosity distribution in the mono-sized pebble bed with fixed wall is agreement well with the Klerk's experimental model [64], which indicates that a relatively reliable results can be obtained in this study.

For binary-sized pebble mixed beds, the lengths of edges along x-axis and y-axis of containers are all equal to 10 times of diameter of large pebbles. The axial local porosities of binary-sized pebble bed with different SR at the maximum packing efficiency state are shown in Fig. 4. The results reveal that the fixed wall also has an obvious effect on the axial local porosity distribution in binary-sized pebble mixed bed. Compared with the mono-sized pebble bed with fixed wall, not only the average porosity in the inner bulk region reduces obviously, but also the volume fraction of the fixed wall influenced regions reduce rapidly in binary-sized pebble bed with fixed wall. When the pebble size ratio is equal to 1, namely mono-sized pebble bed, the fluctuation of local porosity is limited in about $5d_S$ close to the container wall. When the pebble size ratio is equal to 3, the variation of local porosity almost is restricted to the regions closed to the container wall only $3.67d_S$. When the pebble size ratio increases to 5, the change of local porosity is limited in only about $5.83d_S$ close to the side wall. When the pebble size ratio increased to 7, the obvious oscillations of local porosity are confined to less than $8.33d_S$ close to the fixed side wall.

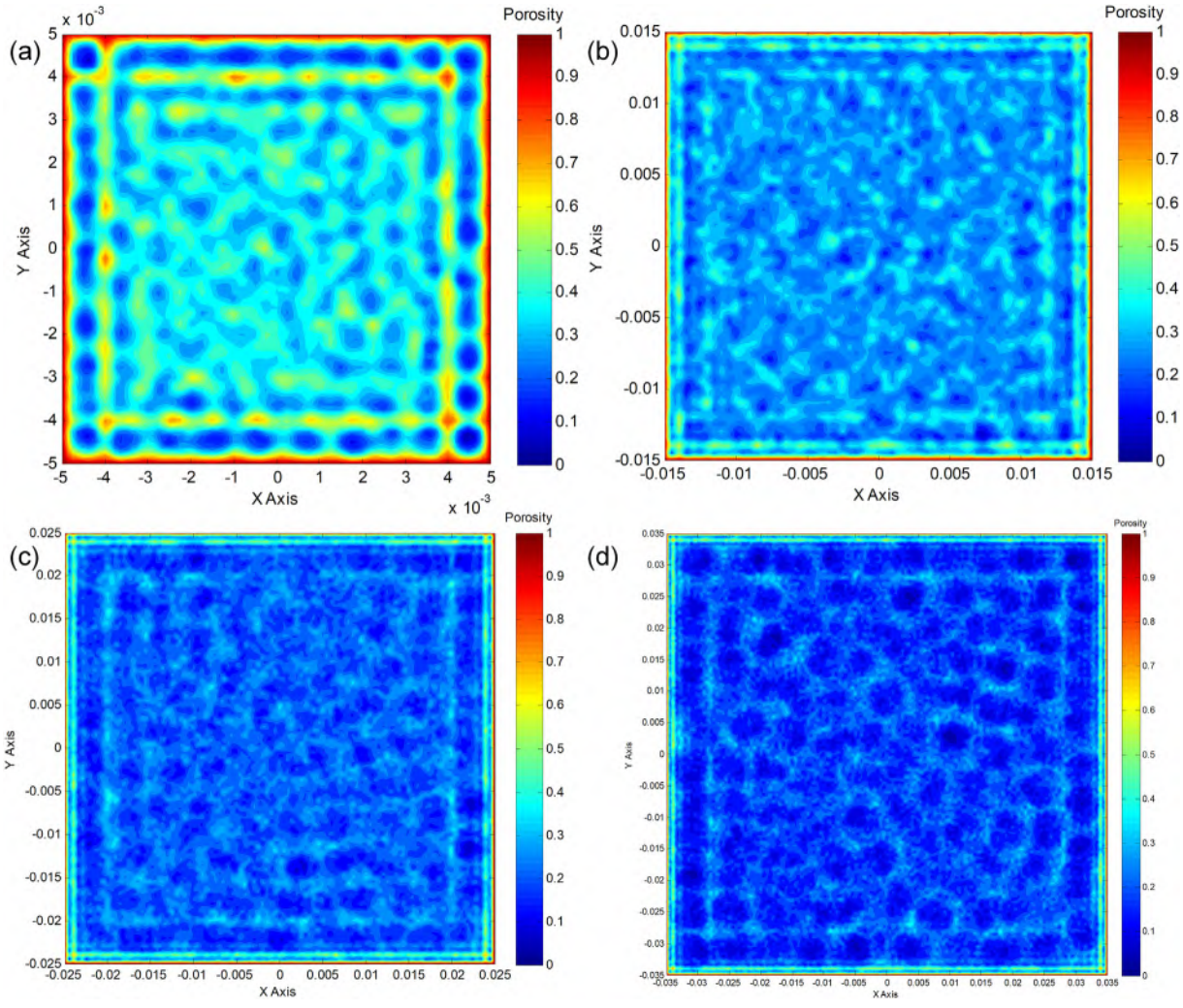

Fig. 5. Porosity distribution of binary-sized pebble bed with fixed wall and different pebble size ratio.

Although the absolute width of wall affected regions get greater with the increase of the pebble size ratio in binary-sized pebble bed, the volume fractions of wall affected regions in whole bed reduce gradually compared with that in the mono-sized pebble bed. Such as, when the pebble size ratios are 1, 3, 5, 7, respectively, the width of porosity fluctuation relative to large pebble diameter, caused by fixed wall effect, is constrained in about $5d_L$, $1.22d_L$, $1.16d_L$, $1.19d_L$ close to the fixed wall. In addition, the contour distribution of local porosity of binary-sized pebble bed with fixed wall and different pebble size ratios at maximum packing efficiency state are shown in Fig. 5. Obvious wall effect in local porosity distribution can be observed from the results. Close to the fixed wall boundary, the distributions of the maximal value and the minimal value of local porosity are stratified parallel to the wall. In the corner region of pebble bed, a crossed-grid distribution can be observed owing to the effect of two fixed side walls, which will bring a reduction of packing fraction and an increase of the porosity. While, in the inner zone of the binary-sized pebble mixed bed, the local porosities are distributed homogeneously and randomly without the effect of fixed wall.

Additionally, to reveal the characterization of pebble packing, the pebble centers were projected into the *x*-*y* plane, as shown in Fig. 6. The wall effect can be observed clearly in both the mono-sized pebble bed and binary-sized pebble mixed bed. It is because that the pebble packing close to fixed wall must conform to the wall shape to achieve equilibrium state. The pebbles adjacent to the wall are contacted with fixed wall in point contact mode, consequently, the maximum porosity can be observed adjacent to the fixed wall. When the distance to fixed wall is about $0.5d_S$, a large number of pebbles gathered, which result in the minimum local porosity and maximum local packing fraction corresponding to the first minimal value of porosity in Fig. 4. With further increase of the distance to fixed wall, the pebble center distribution become more and more uniform and random, and the local porosity tends to a constant value. While, due to the effect of two adjacent fixed wall, the lines formed by the aggregation of pebble center intersect each other, which results in the characterization of the cross-grid distribution of porosity corresponding to the porosity distribution in Figs. 4 and 5.

To summarize, the wall affected regions gradually decrease with the increase of pebble size ratio at the maximum packing efficiency state. The variations of local porosity are contributed to the packing of large pebbles and small pebbles. The packing of large pebbles forms the porous skeleton of the pebble bed, and the small pebbles are fully filled in the gap between the large pebbles. This type of the pebble packing will result in gradual decreases in average porosity of binary-sized pebble mixed bed and in the volume fraction of fixed wall affected region, respectively, with the increase of the pebble size ratio.

In addition, in order to reveal the contribution mechanism of the large pebbles and the small pebbles to the porosity variation near the wall under the influence of the fixed wall effect, we calculated the packing fraction of large pebble, small pebble and all pebbles respectively in binary-sized pebble bed, as shown in Fig. 7. The relation between porosity and packing fraction is as follows: 1 – porosity = packing fraction. The packing fraction of all pebble in pebble bed is the sum of the partial packing fraction of large pebbles and the partial packing fraction of small pebbles. The x-axis was normalized by the diameters of large pebbles (d_L) in Fig. 7b–d. Fig. 7a shows the packing fraction of the

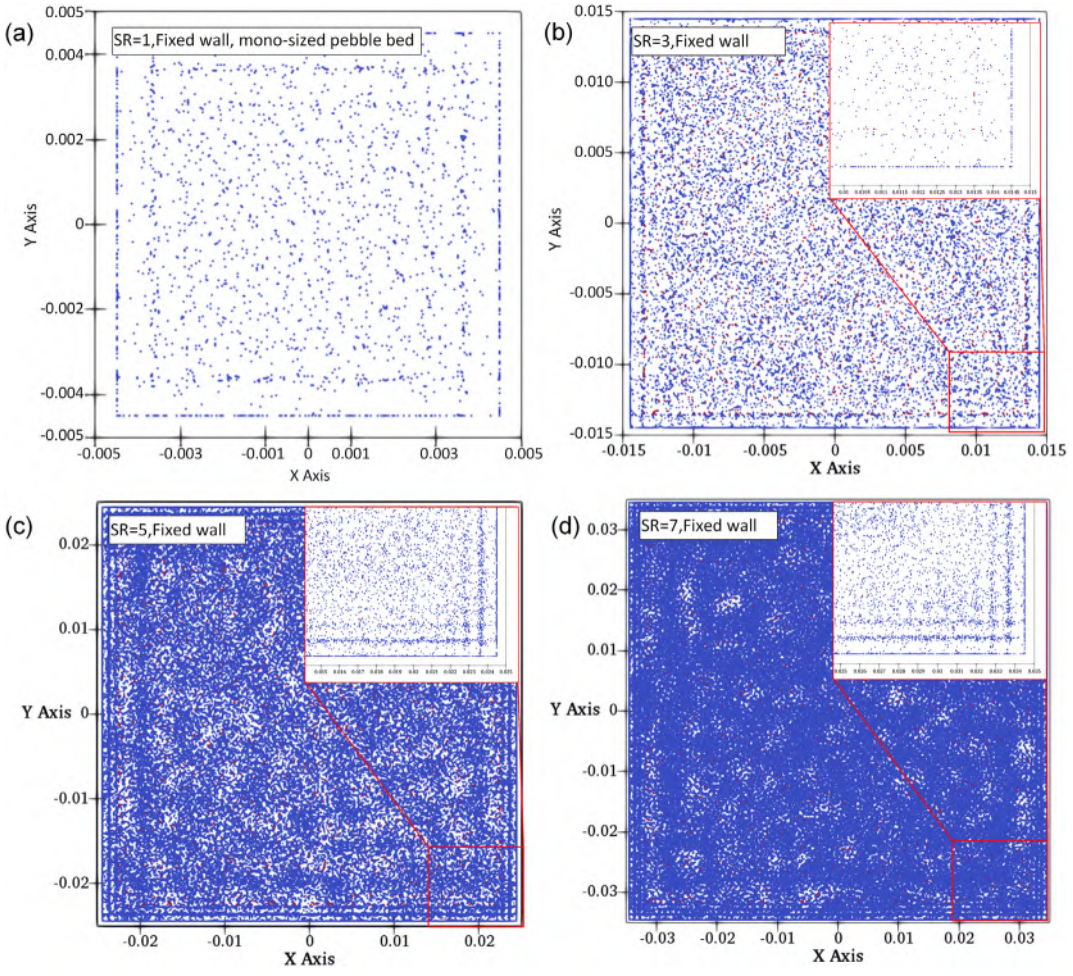

Fig. 6. Pebble center distribution of binary-sized pebble mixed bed with different pebble size ratio.

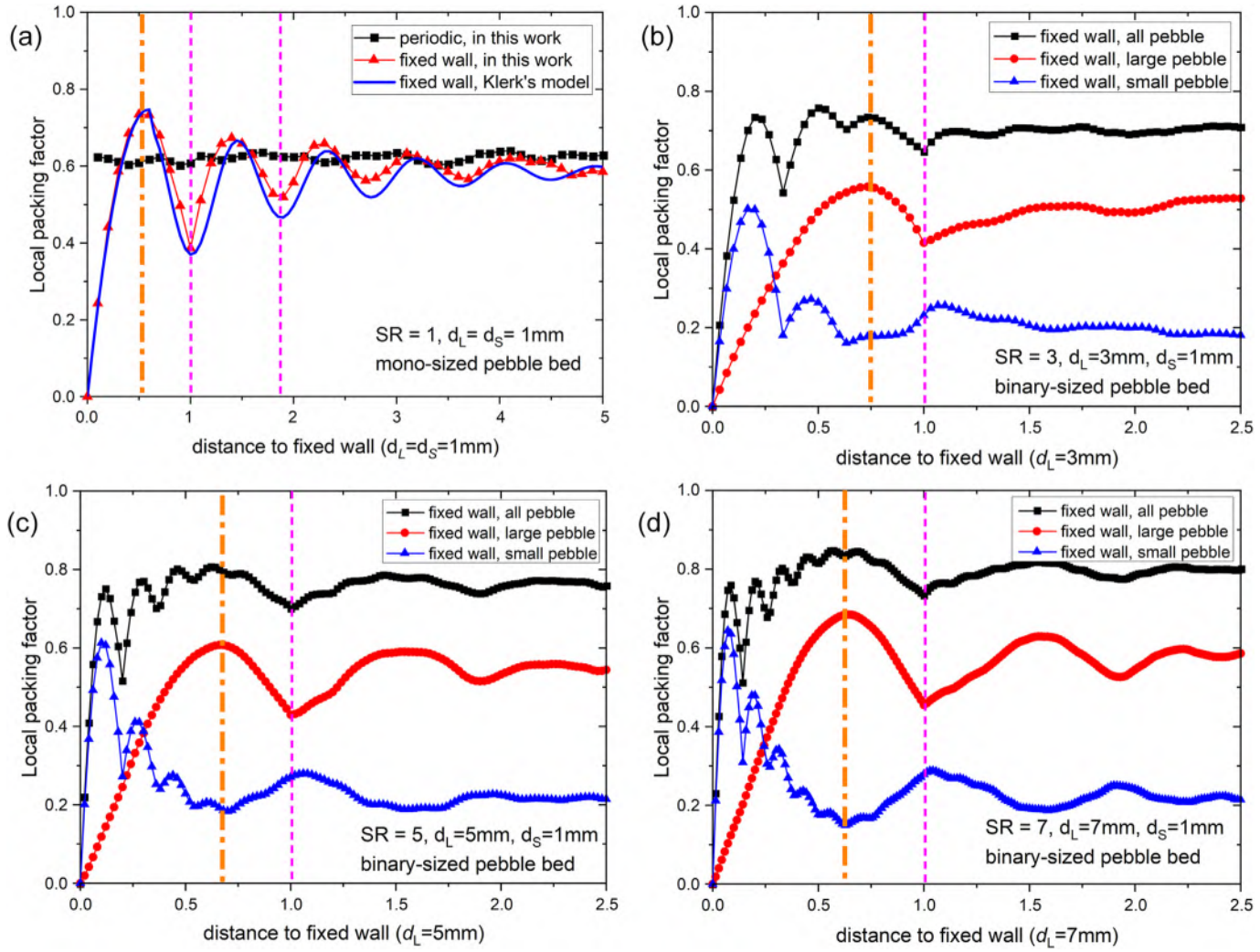

Fig. 7. Effect of pebble size ratio on the local packing fraction in binary-sized pebble bed: (a) SR = 1, $d_L = d_S = 1$ mm, (b) SR = 3, $d_L = 3$ mm, $d_S = 1$ mm, (c) SR = 5, $d_L = 5$ mm, $d_S = 1$ mm, (d) $S_R = 7$, dL = 7 mm, $d_S = 1$ mm.

mono-sized pebble beds (SR = 1, $d_L = d_S = 1$ mm). It can be seen from the results in Fig. 7b–d that the variation of the local packing fraction of the binary-sized pebble bed is mainly determined by the partial packing fraction of large pebbles and the partial packing fraction of small pebbles, respectively. With the increase of the distance to the fixed wall, the contributions of the large pebbles and small pebbles are different. When the distance to fixed wall is less than the radius of the large pebble, $0.5d_L$, the variation of local packing fraction is mainly dominated but the packing of small pebbles, as shown in Fig. 7b–d, the oscillation period of all pebbles is similar to that of the partial packing fraction of small pebbles. For instance, when the SR = 5, there are 3–4 peaks of local packing fraction of whole pebble bed labeled as (■) in Fig. 7c, the profile of the partial packing fraction of small pebbles labeled as (♦) also show 3–4 peaks at the same position. However, when the distance to fixed wall is greater than the $0.5d_L$, the variation characteristics of packing fraction of all pebbles in binary-sized pebble bed is consistent with that of large pebbles, but opposite to that of small pebbles.

For the binary-sized pebble mixed bed, the partial local packing fraction of large pebbles oscillates and decays in the range of $1–1.5d_L$ close to the fixed wall. When the distance to the wall is $1.0d_L$, a minimal value of the partial local packing fraction of large pebbles can be obtained. When the distance is greater than the $1.5d_L$, the partial local packing fraction of large pebbles tends to a constant. However, compared with the maximum of the local packing fraction of mono-sized pebble bed appeared at the distance to the wall of $0.5d_L$, the position of the maximum partial local packing fraction of large pebbles at the maximum packing efficiency state is shifted due to the effect of small pebble packing. With the increase of the SR, the maximum partial local packing fraction gradually approach to the fixed wall. Such as, when the SR =3, the maximum of partial local packing fraction of large pebbles appears at the position about $0.75d_L$ away from the side fixed wall. When the SR increase to 7, the maximum appears at about $0.625d_L$ close to fixed wall.

For the packing of small pebbles in binary-sized pebble mixed bed, there are several oscillation peaks which decrease rapidly when the distance to the fixed wall gradually approach to $1d_L$. The number of the oscillation peaks gradually increases as the SR increases. When SR = 3, 5 and 7, the numbers of the oscillation peaks of partial local packing fractions of small pebbles are equal to 2, 4 and 6, respectively. In addition, when the SR = $1d_L$, a maximal value of partial local packing fraction of small pebbles appears, on the contrary, the partial local packing fraction of large pebbles has a minimal value. With the further increase of the distance to fixed wall, the opposite variation tendency of the partial local packing fraction of large pebble and small pebble can be observed, as shown in Fig. 7, which further verifies that the small pebbles are fully filled in the gaps formed between large pebble at the maximum packing efficiency state. The packing state of entire pebble bed combines the packing characteristics of large pebble and small pebble. The local

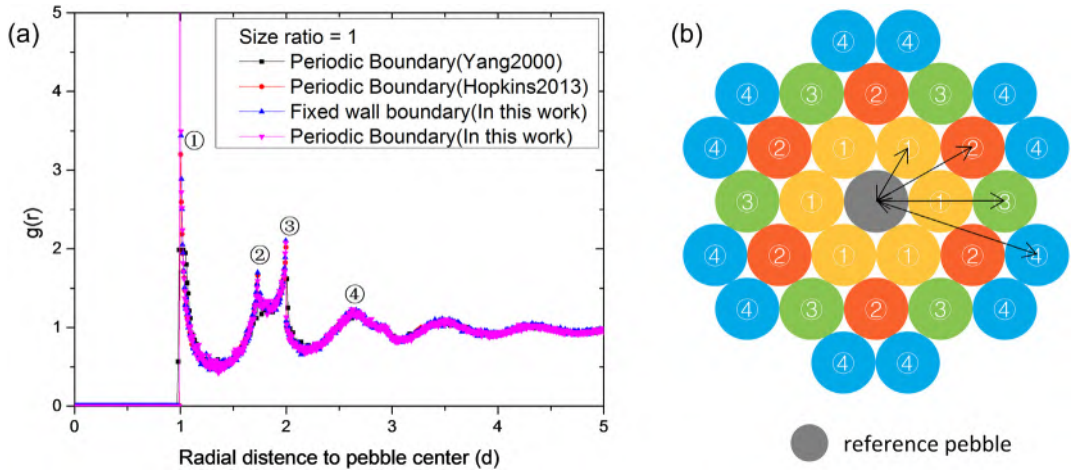

Fig. 8. Radial distribution functions for mono-sized pebbles bed: (a) RDFs, (b) organization (color online).

packing fraction of binary-sized pebble mixed bed is dominated by the partial local packing structures of small pebble and large pebble at the maximum packing efficiency state.

3.2. Effects of pebble size ratio on radial distribution function

Radial distribution function (RDF) is another parameter commonly used to give a well explanation of inner packing structure of pebble bed as it can reveal the useful information about the inter-pebbles radial correlations therein. In other words, The RDF can provide how the density of pebble number varies as a function of the distance r to a given pebbles, which is defined as the probability of discovering one pebble center at a provided distance from the center of a given pebbles [65–67], expressed as $g(r)$ and given by $g(r) = \Delta N(r)/(4\pi r^2 \Delta r \rho_0)$, where $\Delta N\ (r)$ is the number of pebble centers located at the distance between r and $r + \Delta r$ from the center of a given pebble and ρ_0 is the average density of pebble number in the pebble bed. The RDFs in pebble beds are obtained by averaging the RDFs of all similar pebbles. Such as, the RDFs of large pebble are obtained by averaging the RDFs of large pebbles with same diameter in binary-sized pebble bed. And the distance r is normalized by small pebble diameter in the binary-sized pebble bed.

In this work, the RDFs of pebbles in mono-sized pebble beds are compared with the results in literature [65,66] and plotted in Fig. 8a. The RDFs show the split-second peaks in mono-sized pebble beds with fixed wall boundary and periodic boundary, which are agreement well with the previous results reported in Ref. [65, 66]. The boundary conditions almost have no influence on the RDFs. For mono-sized pebble beds, the RDF has been well established [67]. For the random close packing of mono-sized random packed pebble bed, the RDFs displayed a sharp peak

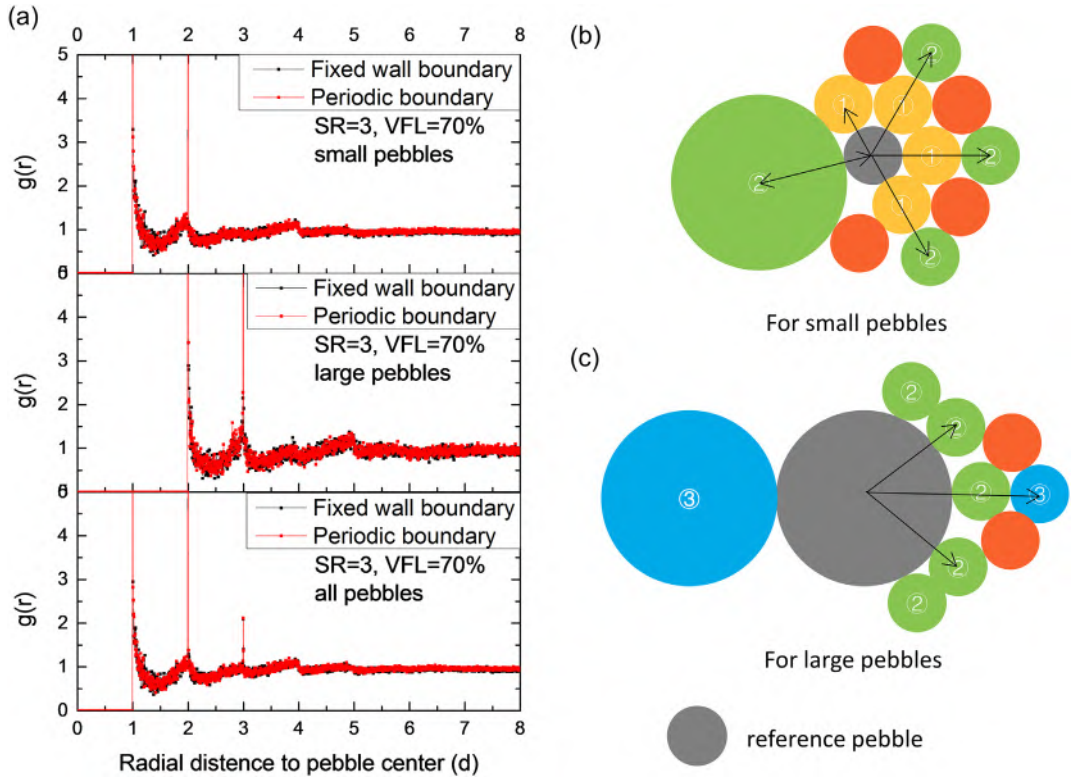

Fig. 9. Radial distribution functions for binary-sized pebble bed with SR = 3 (color online).

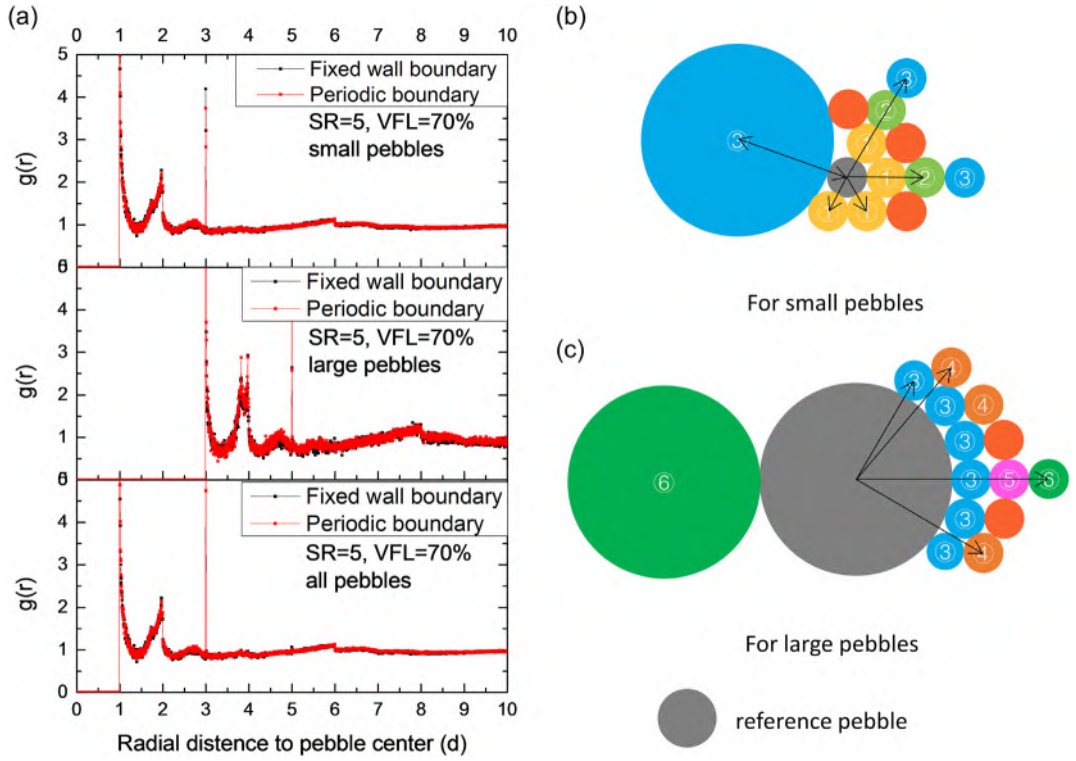

Fig. 10. Radial distribution functions for binary-sized pebble bed with SR = 5 (color online).

at the distance of $r/d = 1$, which is caused by the surrounding pebbles in direct contact. The relatively smaller peaks appeared at the distances to a referenced center pebbles of 1.73, 2 and 2.61 pebble diameters. The distances of the second peak from the centered pebble are $\sqrt{3}$ pebble diameter, the third and the fourth peaks appeared at the distance of $r/d = 2$ and $3\sqrt{3}/2$. The RDFs for the mono-sized pebble beds reveals the organization structures of pebble arrangements [67], as shown in Fig. 8b.

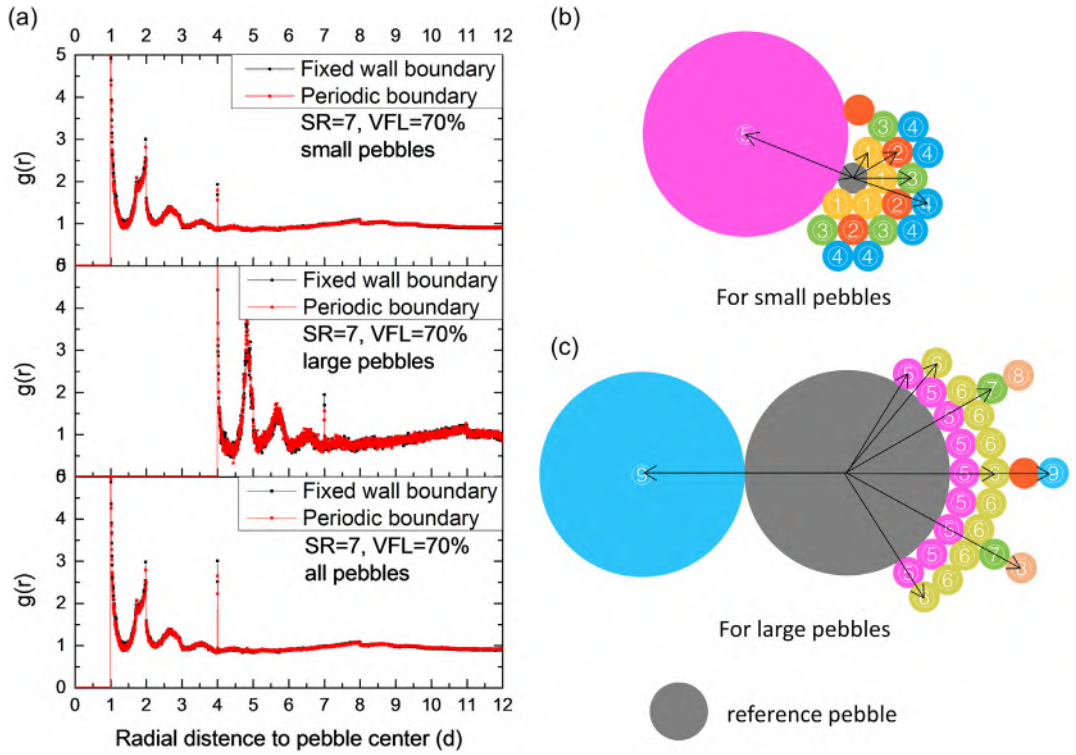

Fig. 11. Radial distribution functions for binary-sized pebble bed with SR = 7 (color online).

For the binary-sized particle mixed bed, Dong et al. [59] investigated the granular crystallization of the 2D binary packing with the SR in the range of 1.03–1.3. For the smaller pebble size of 1.06, the packing of 2D binary particle shows a more ordered packing structures due to at a specific distance from a target particle a certain number of particles are easier to be found [59]. The characteristics of the RDF of 2D binary particle packing are similar to that of the mono-sized pebble bed. Thus, in this work, the RDFs of binary-sized pebble bed in 3D were calculated further with greater pebble size ratio of 3–7. The RDFs of the large pebble, small pebble and whole bed were also compared with that in the mono-sized pebble bed, as plotted in Figs. 9a, 10a and 11a. The radial distance was normalized by the diameter of small pebbles ($d_S = 1$ mm). The presence of the peaks in RDFs indicate the organization structures of the binary-sized pebble packing, as shown in Figs. 9, 10 and 11. The gray pebble is used as the reference pebble. The RDFs and the organization structures for binary-sized pebble mixed beds are obviously different and complex compared that of mono-sized pebble bed.

When SR = 3, the RDFs and the organization of large pebble and small pebble are illustrated in Fig. 9 respectively. For small pebble, the first and the second peaks appeared at the distance to the reference small pebble center of 1d and 2d. The first peak represents the small pebbles touched the reference small pebble. And the second peak was contributed by the large pebbles in directly contact with the reference small pebble and the small pebbles at the distance to the referenced small pebble center of 2d, which were marked by ② in organization in Fig. 9b. While, for large pebble, it was surround by lots of small pebbles.

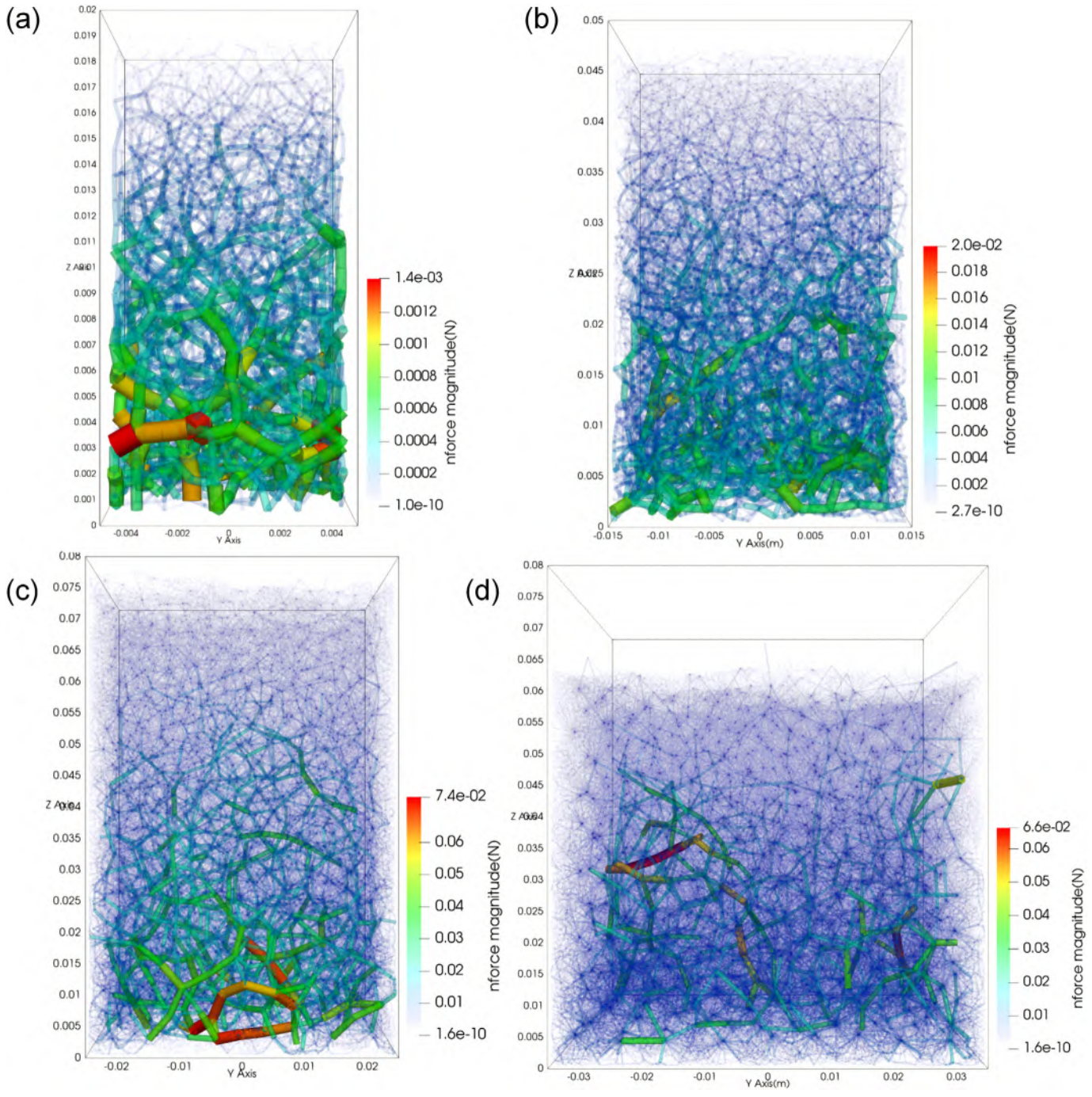

Fig. 12. Contact force chains distribution along the local height in the binary-mixed pebble bed.

So, the first peak in the RDF of large pebble is all contributed by the small pebbles in direct contact with the reference large pebble. The peak appears in the distance from the large particle center of 2d, and the small pebbles are also marked with ② in Fig. 9c. The second peak in the RDF of large pebbles is caused by both the large particles in direct contact with the referenced large pebble and the small pebbles with the distance of 3d, which were marked with ③ in Fig. 9c. However, The RDF of both large and small pebbles showed two distinct peaks, and the second peak didn't show the splitting characteristics compared with the RDF of mono-sized pebble bed. This is mainly because the lattice structure of the small particles is greatly distorted due to the presence of large particles, which affects the uniformity of the packing structure of the mono-sized pebble bed. For the entire binary-sized pebble mixed bed, the RDF showed three distinct peaks. As can be seen from the figure, the RDF of the entire binary-sized pebble bed can be considered as the combination of the RDFs of large pebble and the RDF of small pebble.

When SR = 5, the RDFs and the inner organization structures of the binary-sized pebble bed are shown in Fig. 10. It can be seen from Fig. 10a that the RDF of the small particles have three peaks at the distance of the reference small pebble of 1d, 2d and 3d, respectively. The small pebbles in direct contact with the reference small pebbles result in the first peak, and the second peak was contributed by the small pebbles at the distance to the reference small pebbles of 2d. The combination of the small pebbles at the distance to referenced small pebble of 3d and the large pebbles in contact with the reference small pebble result in the appearance of the third peak. The corresponding organization can be found in Fig. 10b. For large particles, the first peak is only caused by small pebbles that are in contact with the reference large pebbles. The RDF of large pebble exhibits a split-second peak, which is mainly contributed by the surrounding small pebble and the corresponding pebbles are labeled ④ and ⑤ in the organization structures in Fig. 10c.

As can be seen from Fig. 11, when SR = 7, the RDF of small pebbles is similar to the RDF of mono-sized pebble bed and also shows the split-second peaks (labeled ② and ③ in Fig. 11a.). And the difference from mono-sized pebble bed is the fifth peak, which is mainly contributed by the large pebbles in contact with the referenced small pebble. As the SR increase, the other peaks in the RDF of small pebbles will gradually coincide with the RDF of the mono-sized pebble bed, and the split-second peak will be more obvious. This is mainly because small pebbles are filled in the gaps formed between the large pebbles in binary-sized pebble bed. With the increase of SR, the number of small pebbles filled in a single gap is increasing, and the local packing structure of the small pebble in the gaps will become more and more uniform and will gradually approach to the packing structure of the mono-sized pebble bed, and the local lattice distortion that occurs due to the influence of large particles is gradually reduced. Thus, as the SR increases, the RDF of the small pebbles will gradually approach the one of mono-sized pebble bed. From the RDF of the large pebbles, it is clearly show that the four

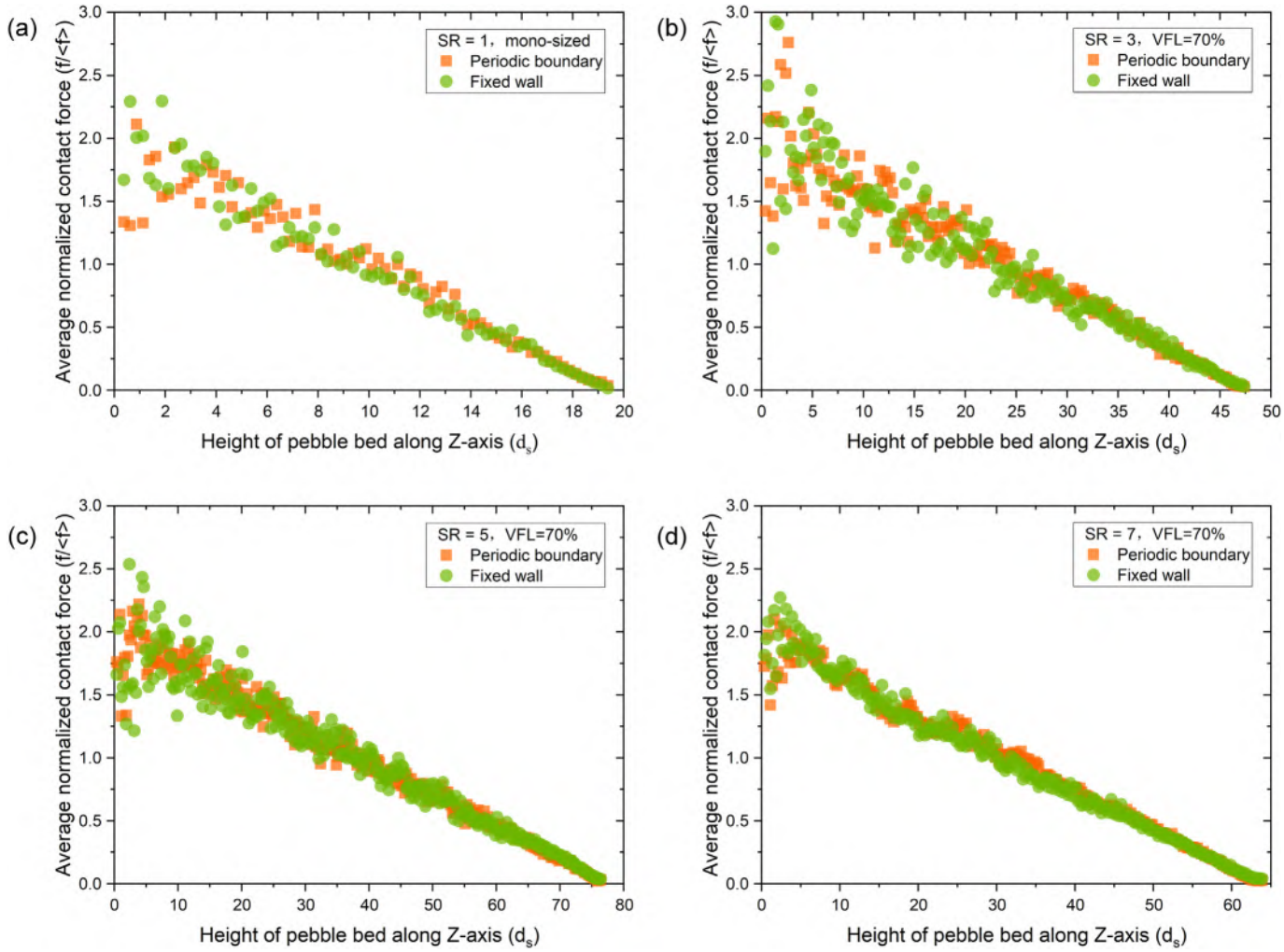

Fig. 13. Position distribution of average contact force along local height (*z*-axis).

peaks in the front are mainly contributed by the small pebbles around the large pebbles. And the fifth peak (marked as ⑨) is mainly caused by both the small pebbles with distance of 7d from the reference large pebble and the large pebbles directly in contact with the reference large pebble.

In addition, with the increase of the SR, the RDF of the whole binary-sized pebble bed will gradually converge with the RDF of small pebbles, which is mainly due to the fact that the RDF of the whole pebble bed is a combination and an average of the RDF of large pebble and the RDF of small pebble. As the SR increases, the number of large pebbles in the unit volume decreases rapidly and the number of small pebbles increases quickly. Thus, the several peaks in the RDF of large pebble were submerged when averaging.

3.3. Effect of pebble size ratio on contact force distribution

3.3.1. Contact force distribution along height

The contact force at each contact point can be obtained in the discrete element method simulation, which provides an opportunity to explore and analyze the contact force distribution in the inner region of binary-sized pebble bed. In this study, the packing of dry pebbles in prismatic containers were modeled and analyzed. The contact force and the gravity were applied in the simulation. The gravity is along the negative *z*-axis. In the pebble bed, if we use a cylinder to connect two contacted pebble centers and use cylinder diameter and color to represent the contact force magnitude, a network of contact force chains will be formed. The force chains play an important role in the pebble packing. The net-shaped framework of the contact force chains keeps the stability of pebble packing and supports the gravity and the external load. The contact force chains distribution in binary-sized pebble bed with different size ratio are shown in Fig. 12. In order to clearly exhibit the strong contact force inside the binary-sized pebble mixed bed, the majority of the weak contact forces have been made transparent. It can be clearly found that the magnitude of the strong contact force gradually decreases along the local heights due to the effect of gravity force. The strong contact force is generally distributed in the lower region of the bed. While, the weak contact force chain runs through the entire binary-sized pebble bed.

In addition, in order to further analyze the contact force, the local averaged contact force along local height is shown in Fig. 13, which was obtained by calculating the average value in a micro volume with a step of $0.5d_S$ height at various local height in the pebble bed. The results in Fig. 13 show that the averaged normalized contact force inside the pebble bed is gradually decreasing with the increase of local height in pebble bed. Close to the bottom wall, the averaged normalized contact force reaches the maximum and always changes around 2 in all of

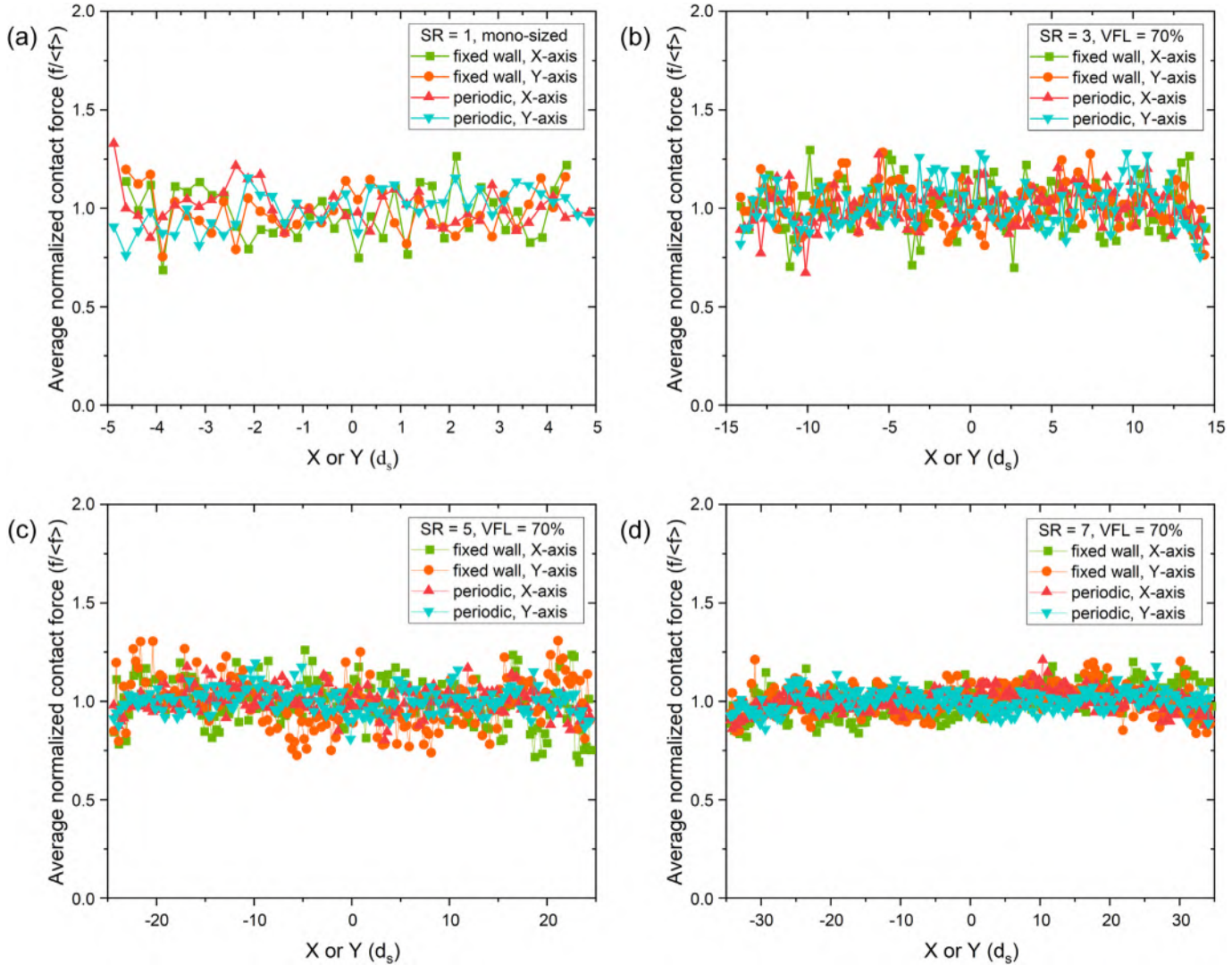

Fig. 14. Position distribution of average contact force along horizontal direction (*x*/*y*-axis).

binary-sized pebble bed. The pebble size ratio and fixed wall seems to have no effect on the averaged normalized contact force near the bottom wall. It is because the friction interaction between pebble and wall and between pebbles can carry part of the gravity force of pebble in the pebble bed. In addition, as shown in Fig. 14, the averaged normalized contact force is always distributed evenly along the horizontal direction due to the relatively isotropic and uniform structures. The fixed wall and the pebble size ratio have few influences on the position distribution of averaged normalized contact force along both the vertical and the horizontal direction.

3.3.2. Probability distribution of contact force

The probability distribution of the normalized contact force in the binary-sized pebble mixed beds were plotted in Fig. 15. It is clearly show that the boundary conditions have little influence on the probability distribution of contact force in both mono-sized pebble beds and binary-sized pebble mixed beds. When SR = 1, the pebble bed can be considered as mono-sized pebble bed. For validation, the probability distributions of contact force in the mono-sized pebble bed are shown in Fig. 15a and compared with the Ngan's Model [68]. The results in this study are clearly consistent with those of the Ngan's Model [68]. The probability density of contact force decreases rapidly with the increase of contact force. Most of the contact forces are smaller than the average contact force (i.e., normalized contact force = 1), and only a small amount of contact forces is much greater than the average contact force, which are in line with the results of contact force chain distribution in Fig. 12. For binary-sized pebble mixed bed, the probability density distributions of the normalized contact force are shown in Fig. 15b–d. The results in Fig. 15 indicate that the probability density of strong contact force in binary-sized pebble mixed bed is greater than that in mono-sized pebble bed owing to contact between large pebble and small pebble and between large pebbles. With the increase of the SR, the pebbles below the large pebbles need greater contact force to carry the gravity of the pebbles above.

In addition, the probability density distribution of binary-sized pebble bed with different pebble size ratio at the maximum packing efficiency state is shown in Fig. 16a and compared that of mono-sized pebble bed. In order to clearly show that difference of probability density distribution in different contact force ranges, the probability density distribution in Fig. 16a was enlarged according to different contact force ranges, which are rescaled the y-axis to clearly display and shown in Fig. 16b, c and d corresponding to the regions (1), (2) and (3) in Fig. 16a. Fig. 16b shows the probability density of the weak force which is smaller than the average contact force. It can be seen from the figure that when the contact force is less than 0.15, the

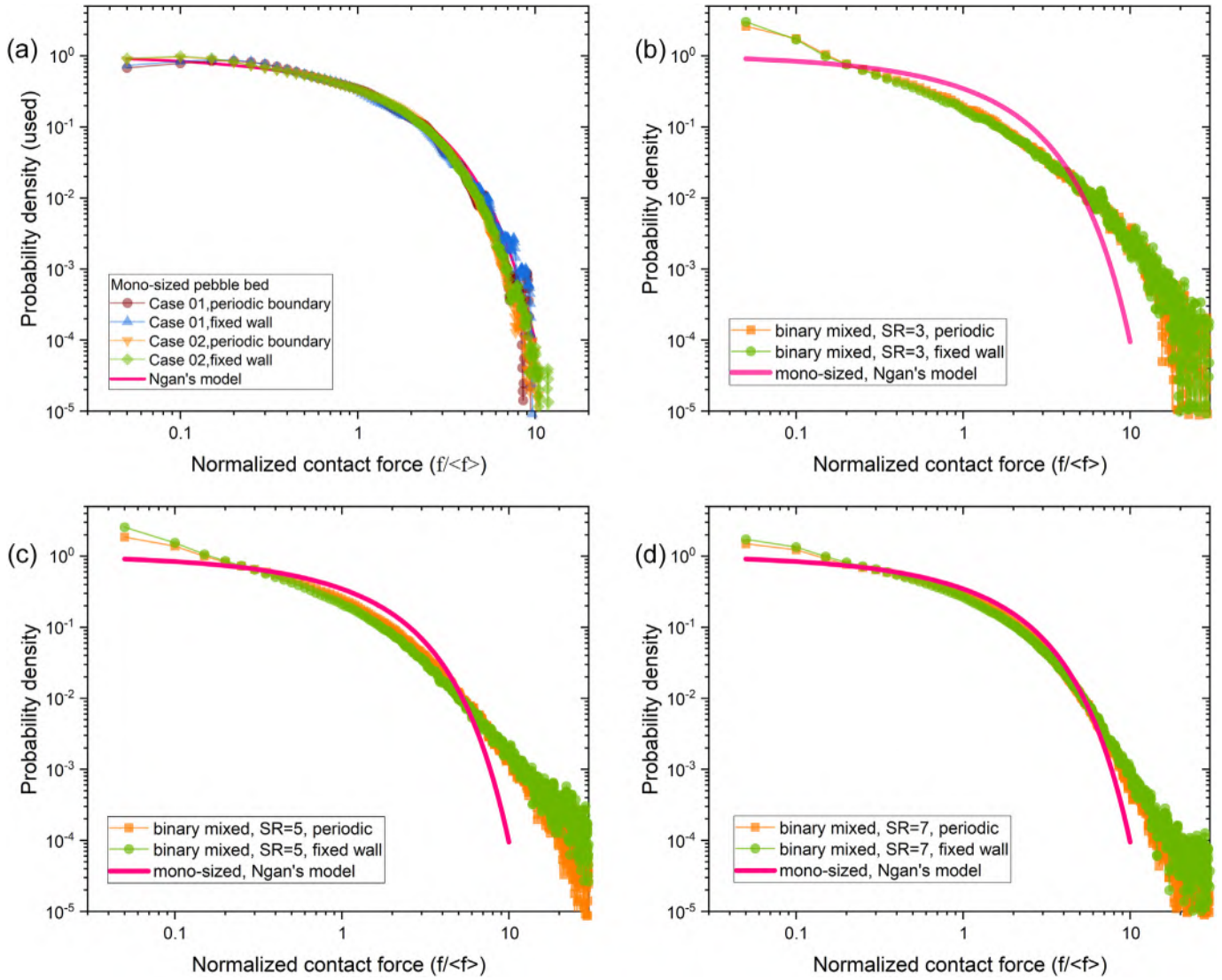

Fig. 15. Effects of pebble size ratio and boundary condition on the probability density distribution of contact force.

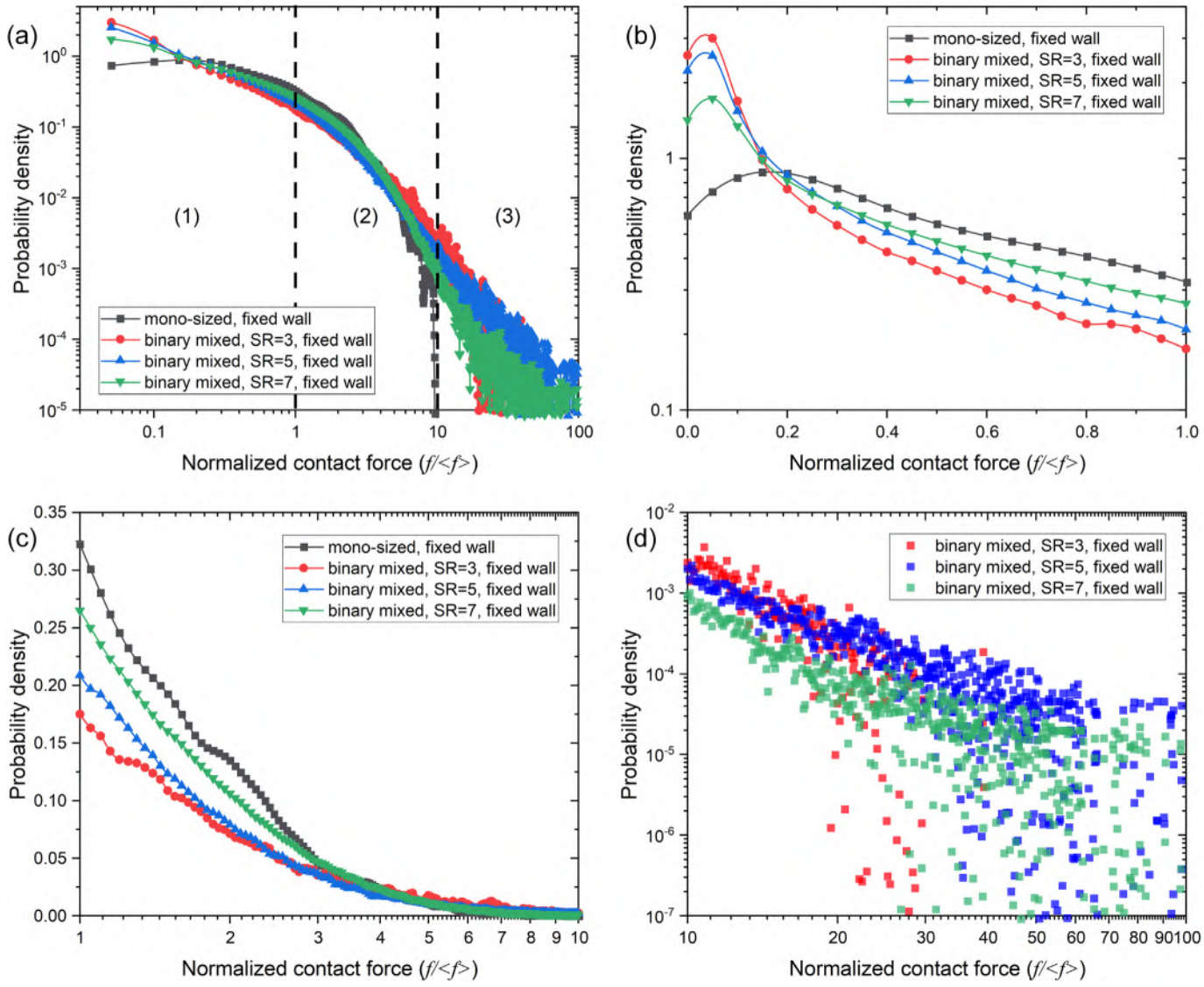

Fig. 16. Effect of pebble size ratio on the probability density distributions of all contact force.

probability density of contact force in the binary-sized pebble mixed bed is significantly higher than that in the mono-sized pebble bed and decreases with the increase of the pebble size ratio. It might because at the maximum packing efficiency state, the small pebbles are fully filled in the void space between the large pebbles, the gravity and external load in the pebble bed are mainly carried by the strong contact force between the large pebbles. Thus, most of the contact forces between the small particles are smaller weak contact force. However, when the normalized contact force is greater than 0.2, an opposite variation tendency is observed. That is to say, the probability density of contact force of mono-sized pebble bed is greater than that of binary-sized pebble bed. With the increase of particle size ratio, the probability density of contact force of binary-sized pebble bed increases, and a similar change is observed from Fig. 16c. The difference might be attributed to the contact mode in binary-sized pebble bed. For example, the contact forces in binary-sized pebble bed are formed by small-small pebble contact, small-large pebble contact and large-large pebble contact. A relatively strong contact force is always obtained by large-large contact and small-large contact. A relative weak contact force exists in the contact between small pebbles. When the normalized contact force is larger than 10, there is almost no normalized contact force greater than 10 in the mono-sized pebble bed. However, in the binary-sized pebble mixed bed, there are many super strong contact forces, which are very important for analyzing the crushing characteristics of the pebbles in the binary-sized pebble mixed bed. Moreover, with the increase of pebble size ratio, the maximum contact force inside binary-sized pebble bed increases gradually, but the probability density of super strong contact force decreases gradually, which is mainly due to the decrease of the number of large pebbles.

In general, there are several contacts for each individual pebble in the binary–sized pebble bed, which will result in several contact force of every pebble. For each individual pebble, the maximum contact force is very important due to that if the maximum contact force is greater than the crush load, the pebble might break or crack [69,70]. Therefore, the maximum contact force of each pebble was analyzed in this study. The probability density distributions of the maximum contact force of each pebble in binary pebble bed with different pebble size ratio are shown in Fig. 17a. Similarly, in order to clearly display the probability density of different ranges of contact force, the regions (1), (2) and (3) in Fig. 17a are enlarged and shown in Fig. 17b, c and d, respectively. It can be seen from the results that even if the maximum contact force of each pebble in the binary-sized pebble bed, most of the contact force is still smaller than the average contact force, that is to say, most of the pebbles in the pebble bed will not be broken under the

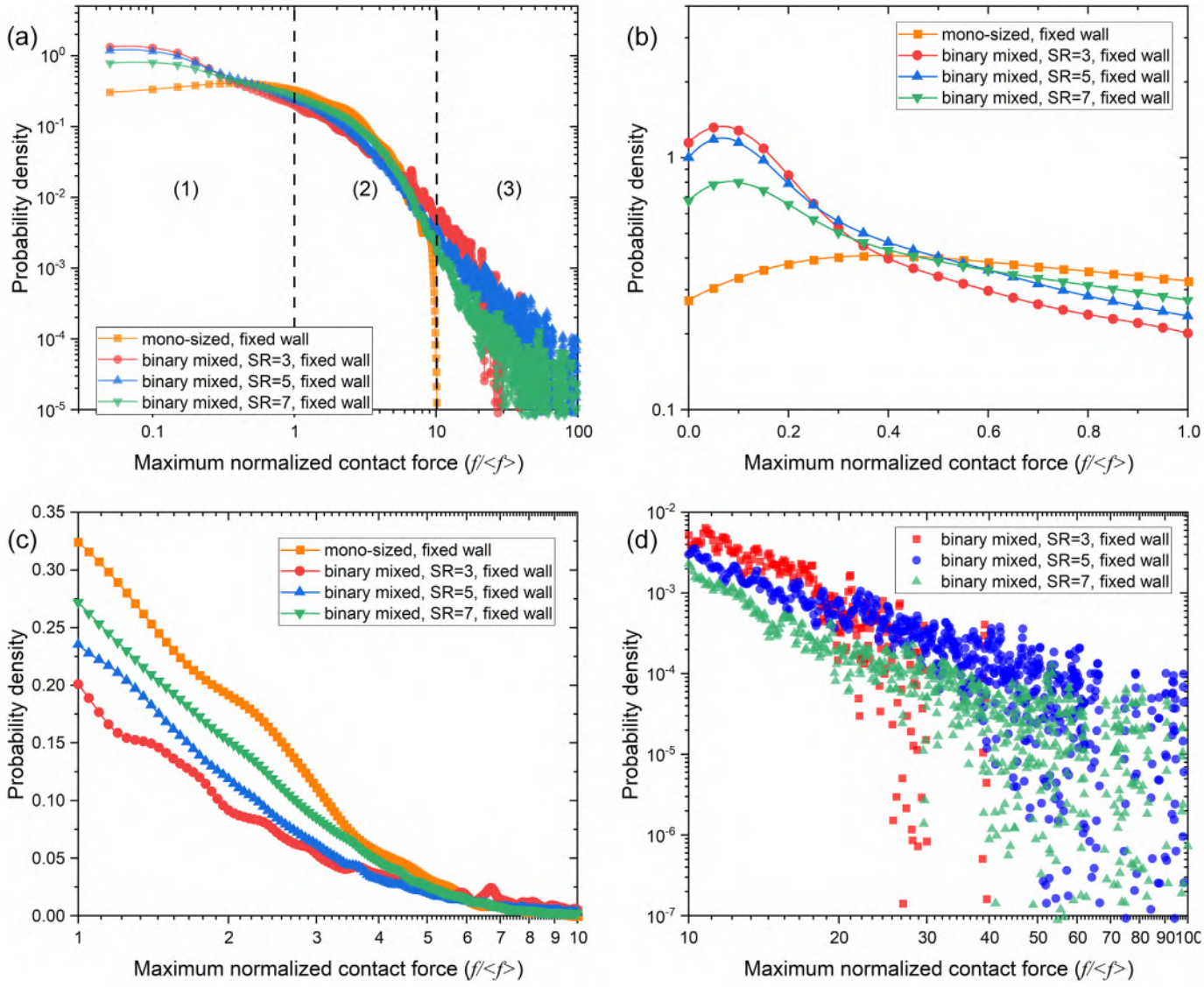

Fig. 17. Effect of pebble size ratio on the probability density distributions of maximum contact force of each pebble.

natural packing of gravity. In addition, compared with the probability density distribution of all contact force, the probability density of the maximum contact force of each pebble, which is less than the average contact force, is reduced. While, for the probability density of the maximum contact force of each pebble, the probability density increases compared with that of all contact force when the normalized contact force is greater than 10, which further indicates that pebbles with super strong contact force are likely to break up in the binary-sized pebble bed, especially when the contact force exceed the crush load of pebbles in pebble bed suffering the external load.

4. Conclusion

At the maximum packing efficiency state, the packing structures and the contact force distributions of binary-sized pebble beds with fixed wall and periodic boundary were investigated by the DEM simulation. The evolution of the distribution of packing fraction and porosity, radial distribution function and the contact force were analyzed. The effect of the fixed wall and pebble size ratio on the porosity distribution were discussed in detail. In addition, the influence of the pebble size ratio on the radial distribution function and the contact force were also studied. From the results gained in this study, it is clearly and obviously show that the boundary condition (fixed wall and periodic boundary) has a great effect on the local porosity distribution in binary-sized pebble bed. Fixed wall will result a relative higher average porosity and an obvious wall effect in local porosity distribution. Compared with the mono-sized pebble bed, the volume fraction of wall affected region is reduced obviously by using the binary-sized pebble packing with larger pebble size ratio. Furthermore, the fixed wall has little effect on the radial distribution function and contact force. However, the radial distribution function and the contact force distribution in binary-sized pebble bed are significantly affected by pebble size ratios. With the increase of SR, the RDFs of the whole pebble beds are consistent with the RDFs of small pebbles, and they also approach to the RDFs of mono-sized pebble bed. In addition, with the increase of the pebble size ratio, a higher contact force can be obtained in binary-sized pebble beds.

Declaration of Competing Interest

The authors declare that they have no known competing financial interests or personal relationships that could have appeared to influence the work reported in this paper.

Acknowledgments

This study is supported by the National Natural Science Foundation of China under Grant No. 11905047, by the National Key Research and Development Program of China under Grant No. 2017YFE0300602, by Sichuan Science and Technology Program from Science & Technology Department of Sichuan Province of China under Grant No. 2018JZ 0014. The simulation work was supported by HPC Platform, Southwestern Institute of Physics.

References

[1] X. Chen, et al., The packing fraction of the pebble bed in molten salt reactor, Ann. Nucl. Energy 122 (2018) 118–124.
[2] C.H. Rycroft, et al., Analysis of granular flow in a pebble-bed nuclear reactor, Phys. Rev. E 74 (2006), 021306, .
[3] K. Feng, et al., Current progress of Chinese HCCB TBM program, Fusion Eng. Des. 109-111 (2016) 729–735.
[4] S. Cui, et al., Evaluation and optimization of tritium breeding, shielding and nuclear heating performances of the helium cooled solid breeder blanket for CFETR, Int. J. Hydrogen Energ. 42 (2017) 24263–24277.
[5] X. Wu, et al., Design optimization and analysis of CN HCCB TBM-set, Fusion Eng. Des. 136 (2018) 839–846.
[6] S. Cui, et al., Numerical research on the neutronic/thermal-hydraulic/mechanical coupling characteristics of the optimized helium cooled solid breeder blanket for CFETR, Fusion Eng. Des. 114 (2017) 141–156.
[7] L. Chen, et al., Investigation of the packing structure of pebble beds by DEM for CFETR WCCB, J. Nucl. Sci. Technol. 53 (2016) 803–808.
[8] Y. Feng, et al., Effects of bed dimension, friction coefficient and pebble size distribution on the packing structures of the pebble bed for solid tritium breeder blanket, Fusion Eng. Des. 163 (2021) 112156.
[9] B. Gong, et al., Effect of pebble size distribution and wall effect on inner packing structure and contact force distribution in tritium breeder pebble bed, Energies 14 (2021) 449.
[10] B. Gong, et al., Discrete element modeling of pebble bed packing structures for HCCB TBM, Fusion Eng. Des. 121 (2017) 256–264.
[11] B. Gong, et al., Numerical investigation of the pebble bed structures for HCCB TBM, Fusion Eng. Des. 136 (2018) 1444–1451.
[12] J. Chen, et al., FW and blanket technology development progress at SWIP, J. Fusion Energ. 40 (2021) 10.
[13] X. Wang, et al., Current design and R&D progress of the Chinese helium cooled ceramic breeder test blanket system, Nucl. Fusion 59 (7) (2019), 076019, .
[14] B. Gong, et al., Investigation of packing behavior of pebble bed in solid tritium breeder blanket, Nucl. Fusion Plasma Phys. 38 (04) (2018) 420–427.
[15] B. Gong, et al., Numerical modeling packing structures of Li4SiO4 pebble bed for HCCB-TBM, Nucl. Fusion Plasma Phys. 37 (02) (2017) 173–180.
[16] B. Gong, et al., Experimental investigation of the effect of particle size on the effective thermal properties of particle beds, J. Eng. Thermophys. 40 (5) (2019) 1151–1159.
[17] S. Pupeschi, et al., Effective thermal conductivity of advanced ceramic breeder pebble beds, Fusion Eng. Des. 116 (2017) 73–80.
[18] S. Pupeschi, et al., Experimental investigation of thermal diffusivity and heat capacity of ceramic breeder beds, J. Nucl. Mater. 518 (2019) 400–408.
[19] M.H.H. Kolb, et al., Enhanced fabrication process for lithium orthosilicate pebbles as breeding material, Fusion Eng. Des. 86 (2011) 2148–2151.
[20] D. Sohn, et al., Numerical prediction of packing behavior and thermal conductivity of pebble beds according to pebble size distributions and friction coefficients, Fusion Eng. Des. 137 (2018) 182–190.
[21] M.D. Donne, et al., Experimental investigations on the thermal and mechanical behaviour of a binary beryllium pebble bed, Fusion Eng. Des. 49-50 (2000) 521–528.
[22] R.K. Annabattula, et al., Mechanics of binary and polydisperse spherical pebble assembly, Fusion Eng. Des. 87 (2012) 853–858.
[23] A.S. Clarke, et al., Numerical simulation of the dense random packing of a binary mixture of hard spheres: amorphous metals, Phys. Rev. B 35 (1987) 7350–7356.
[24] E. Yazdani, et al., DEM simulation of heat transfer of binary-sized particles in a horizontal rotating drum, Granul. Matter 21 (2018) 6.
[25] J. Reimann, et al., Mechanical behavior of monosized and binary beryllium pebble beds, Fusion Technol. 38 (2017) 299–309.
[26] X. An, et al., DEM simulation of binary sphere packing densification under vertical vibration, Part. Sci. Technol. 36 (2017) 672–680.
[27] A.R. Fuggle, et al., Size effects on the void ratio of loosely packed binary particle mixtures, Geo-Congress 2014 Technical Papers, American Society of Civil Engineers, Reston, VA 2014, pp. 129–138.
[28] X. An, et al., Packing densification of binary mixtures of spheres and cubes subjected to 3D mechanical vibrations, Appl. Phys. A-Mater. 118 (2014) 151–162.
[29] J. Yang, et al., DEM investigation of shear flows of binary mixtures of non-spherical particles, Chem. Eng. Sci. 202 (2019) 383–391.
[30] Y. Lee, et al., Numerical investigation of mechanical and thermal characteristics of binary-sized pebble beds using discrete element method, Fusion Eng. Des. 146 (2019) 2285–2291.
[31] R.K. Desu, et al., Mechanics of binary crushable granular assembly through discrete element method, Nucl. Mater. Energy 9 (2016) 237–241.
[32] L. Liu, et al., Determining random packing density and equivalent packing size of superballs via binary mixtures with spheres, Chem. Eng. Sci. 202 (2019) 270–281.
[33] H.A.C.K. Hettiarachchi, et al., Effect of vibration frequency, size ratio and large particle volume fraction on packing density of binary spherical mixtures, Powder Technol. 336 (2018) 150–160.
[34] W. Zhou, et al., Effects of particle size ratio on the macro- and microscopic behaviors of binary mixtures at the maximum packing efficiency state, Granul. Matter 18 (2016) 81.
[35] L. Meng, et al., Packing properties of binary mixtures in disordered sphere systems, Particuology 16 (2014) 155–166.
[36] K.D.L. Kristiansen, et al., Simulation of random packing of binary sphere mixtures by mechanical contraction, Phys. A 358 (2005) 249–262.
[37] D. Mandal, et al., Void fraction and effective thermal conductivity of binary particulate bed, Fusion Eng. Des. 88 (2013) 216–225.
[38] R.S. Farr, et al., Close packing density of polydisperse hard spheres, J. Chem. Phys. 131 (2009) 244104.
[39] Y. Gan, et al., Computer simulation of packing structure in pebble beds, Fusion Eng. Des. 85 (2010) 1782–1787.
[40] J. Wiącek, et al., Effective elastic properties and pressure distribution in bidisperse granular packings: DEM simulations and experiment, Arch. Civ. Mech. Eng. 17 (2017) 271–280.
[41] C.S. Chang, et al., A nonlinear packing model for multi-sized particle mixtures, Powder Technol. 336 (2018) 449–464.
[42] M. Reisi, et al., Computer simulation-based method to predict packing density of aggregates mixture, Adv. Powder Technol. 29 (2018) 386–398.
[43] Y. Yuan, et al., Coupling effects of particle size and shape on improving the density of disordered polydisperse packings, Phys. Rev. E 98 (2018), 042903, .
[44] O. Koutný, et al., Modelling of packing density for particle composites design, Proc. Eng. 151 (2016) 198–205.
[45] V. Baranau, et al., Random-close packing limits for monodisperse and polydisperse hard spheres, Soft Matter 10 (2014) 3826–3841.
[46] V. Wong, et al., A 3-parameter model for packing density prediction of ternary mixes of spherical particles, Powder Technol. 268 (2014) 357–367.
[47] G. Roquier, A theoretical packing density model (TPDM) for ordered and disordered packings, Powder Technol. 344 (2019) 343–362.
[48] R.P. Zou, et al., Packing density of binary mixtures of wet spheres, J. Am. Ceram. Soc. 84 (2001) 504–508.
[49] S.M.K. Rassouly, The packing density of perfect binary mixtures, Powder Technol. 103 (1999) 145–150.
[50] I. Biazzo, et al., Theory of amorphous packings of binary mixtures of hard spheres, Phys. Rev. Lett. 102 (2009) 195701.
[51] J. Reimann, et al., X-ray tomography investigations of mono-sized sphere packing structures in cylindrical containers, Powder Technol. 318 (2017) 471–483.
[52] W. Dai, et al., Modes of wall induced granular crystallisation in vibrational packing, Granul. Matter 21 (2019) 26.
[53] W.V. Antwerpen, et al., A review of correlations to model the packing structure and effective thermal conductivity in packed beds of mono-sized spherical particles, Nucl. Eng. Des. 240 (2010) 1803–1818.
[54] J. von Seckendorff, O. Hinrichsen, Review on the structure of random packed-beds, Can. J. Chem. Eng. 1 (2021) 30.
[55] A. Simoni, et al., The direct shear strength and dilatancy of sand-gravel mixtures, Geotech. Geol. Eng. 24 (3) (2006) 523–549.
[56] C.S. Chang, et al., Dominant grains network and behavior of sand-silt mixtures: stress-strain modeling, Int. J. Numer. Anal. Met. 37 (2013) 2563–2589.
[57] D. Simpson, et al., Behavioral thresholds in mixtures of sand and kaolinite clay, J. Geotech. Geoenviron. 142 (2016), 04015073, .
[58] J. Reimann, et al., 3d tomography analysis of the packing structure of spherical particles in slender prismatic containers, Int. J. Mater. Res. 111 (1) (2020) 65–77.
[59] M. Dong, et al., Morphological characterisation of 2D packing with bi-disperse particles, Int. J. Adv. Eng. Sci. Appl. Math. 13 (1) (2021) 89–97.
[60] P. Cundall, et al., A discrete numerical model for granular assemblies, Géotechnique 29 (1979) 47–65.
[61] LIGGGHTS, (R)-Public Documentation, Version 3.X, Available online http://www.liggghts.com.
[62] H. Liao, et al., Recent progress of R&D activities on reduced activation ferritic/martensitic steel (CLF-1), Fusion Eng. Des. 147 (2019) 111235.
[63] R.K. McGeary, Mechanical packing of spherical particles, J. Am. Ceram. Soc. 44 (10) (1961) 513–522.
[64] A.D. Klerk, Voidage variation in packed beds at small column to particle diameter ratio, AICHE J. 49 (2003) 2022–2029.
[65] R.Y. Yang, et al., Computer simulation of the packing of fine particles, Phys. Rev. E 62 (2000) 3900–3908.
[66] A.B. Hopkins, et al., Disordered strictly jammed binary sphere packings attain an anomalously large range of densities, Phys. Rev. E 88 (2013), 022205, .
[67] J. Wiącek, Geometrical parameters of binary granular mixtures with size ratio and volume fraction: experiments and DEM simulations, Granul. Matter 18 (2016) 42.
[68] A.H.W. Ngan, On distribution of contact forces in random granular packings, Phys. A. 339 (2004) 207–227.
[69] Y. Gan, et al., Crush probability analysis of ceramic breeder pebble beds under mechanical stresses, J. Nucl. Mater. 417 (2011) 706–709.
[70] S. Wang, et al., Effect of packing structure on mechanical properties of the pebble beds and the probability of particle crushing, Fusion Eng. Des. 162 (2021) 112137.